



Geochronology (zircon U-Pb, Hf, O isotopes), provenance analysis, and tectonic setting of the Paleoproterozoic Karrat Group and supracrustal rocks of the Rinkian fold belt, West Greenland

Camille A. Partin^{a,*}, Brayden S. McDonald^a, Michael McConnell^a, Kristine Thrane^c, D. Graham Pearson^b, Chiranjeeb Sarkar^b, Yan Luo^b, Richard A. Stern^b

^a University of Saskatchewan, Department of Geological Sciences, Saskatoon, SK S7N 5E2, Canada

^b University of Alberta, Department of Earth & Atmospheric Sciences, Edmonton, Alberta T6G 2E3, Canada

^c Geological Survey of Denmark and Greenland, Øster Voldgade 10, 1350 Copenhagen, Denmark

ARTICLE INFO

Article history:

Received 24 January 2024

Revised 21 June 2024

Accepted 22 July 2024

Available online 23 July 2024

Handling Editor: Andrea Festa

Keywords:

U-Pb geochronology

Hf isotopes

Zircon

Rae craton

Trans-Hudson orogen

ABSTRACT

We use zircon U-Pb, Hf and O isotopes to constrain the depositional ages and provenance of metasedimentary rocks of the Paleoproterozoic Karrat Group of West Greenland and to understand the tectonic processes leading to basin development on the eastern Rae craton. An older supracrustal assemblage (Qeqertarsuaq complex) deposited after ca. 2.6 Ga is separated by an unconformity with a younger supracrustal assemblage (the Karrat Group). The Qaarsukassak Formation at the base of the Karrat Group was deposited after ca. 2.0 Ga, with dominantly Archean age modes. The youngest siliciclastic rocks (Nûkavsak and Mârmorilik formations) in the Karrat Group have maximum depositional ages ranging from ca. 1980 to 1950 to 1900 Ma and contain dominant detrital zircon age modes between ca. 2.50 and 1.93 Ga. A ca. 1.92 Ga supracrustal assemblage referred to as the northern domain (Karrat Group, *sensu lato*) is geographically separated from the Karrat Group (*sensu stricto*) by the Prøven igneous complex. The stratigraphy and detrital zircon profiles are compared to broadly coeval sedimentary units on the Rae craton and a unifying model of their deposition is presented. The Rae craton is the dominant detritus source; initially these sources were mostly local, changing to a mix of local and distal sources including the western Rae craton. The tectonic setting of the Karrat basin transitioned from extensional to convergent to collisional during its basin evolution, reflecting Wilson cycle phases within an epeiric sea. Accordingly, zircon Hf isotopes in our dataset track the evolution of the opening and closing of the Manikewan Ocean. Detrital zircon Hf isotopes in our dataset reveal a greater proportion of juvenile detritus (especially ca. 2.15–1.95 Ga) than is known from the currently exposed crustal record, pointing to the importance of the detrital zircon record for understanding Paleoproterozoic crustal and tectonic evolution.

© 2024 The Authors. Published by Elsevier B.V. on behalf of International Association for Gondwana Research. This is an open access article under the CC BY-NC-ND license (<http://creativecommons.org/licenses/by-nc-nd/4.0/>).

1. Introduction

The Karrat Group is a Paleoproterozoic supracrustal sequence that crops out over several hundred kilometers along the coast of central West Greenland (Fig. 1) and unconformably overlies Archean rocks of the Rae craton (Henderson and Pulvertaft, 1987). Reconstructing the age, stratigraphy, and depositional environments of the Karrat Group provides an opportunity to better understand the basin tectonic evolution prior to, and during, orogeny related to the Trans-Hudson and Rinkian orogens and the

building of proto-Laurentia. Within the eastern Rae craton, Paleoproterozoic supracrustal sequences that were deposited prior to the Trans-Hudson orogen include the Piling, Penrhyn, and Hoare Bay groups, located in eastern Canada, and the Karrat and Anap nûna groups, located in West Greenland.

Early work postulated that the Piling, Penrhyn, and Karrat groups were correlative, based on similarities in lithostratigraphy and timing of deformation by ca. 1.9–1.8 Ga orogenic events (Jackson and Taylor, 1972; Kalsbeek et al., 1998). Mapping and research initiatives led by the Geological Survey of Canada (e.g., Corrigan et al., 2001) and the Geological Survey of Denmark and Greenland (e.g., Rosa et al., 2018) have led to a greater understanding of the stratigraphy, age, and tectonic history of the supracrustal

* Corresponding author.

E-mail address: camille.partin@usask.ca (C.A. Partin).

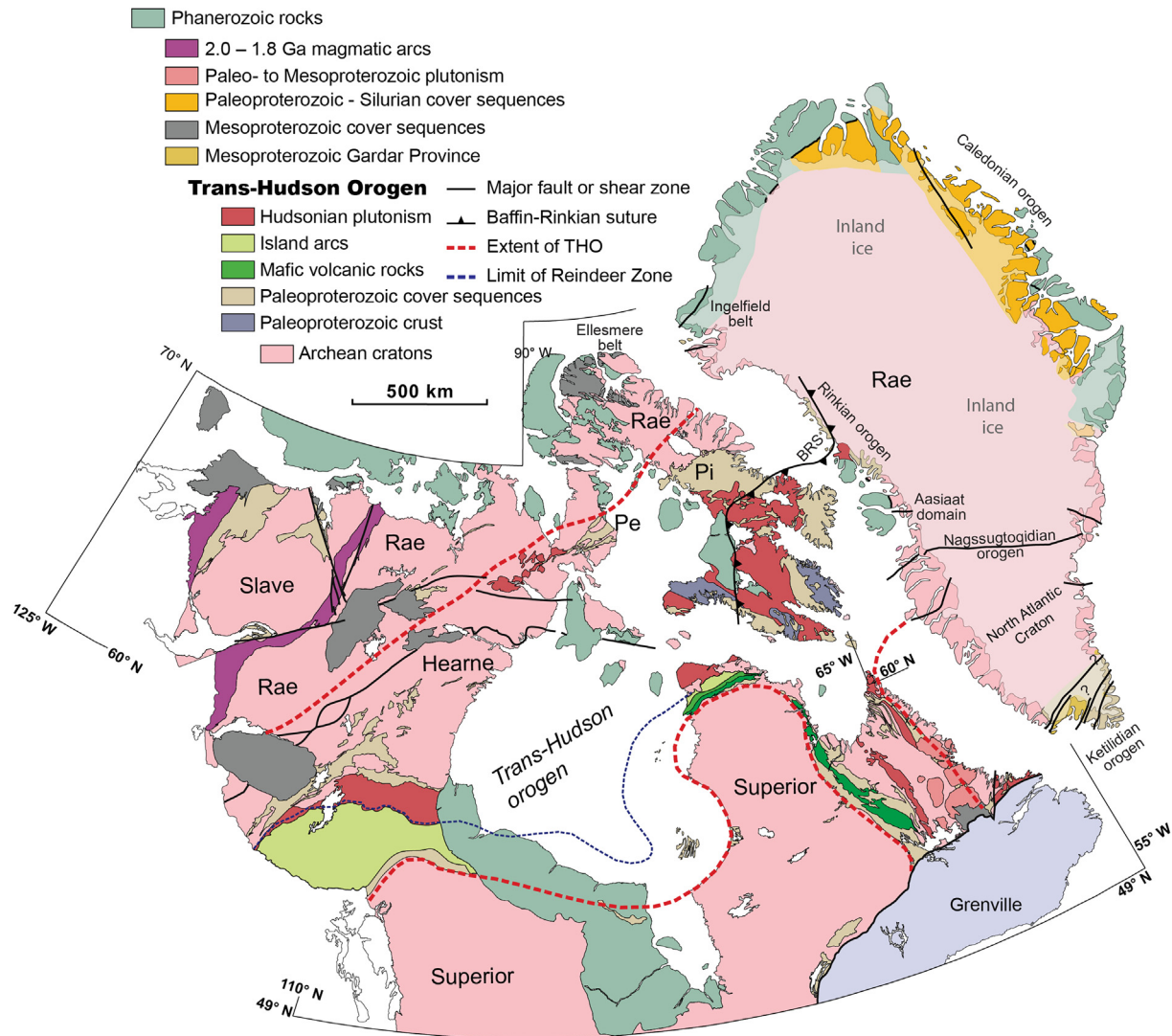


Fig. 1. Geological map of Canada-Greenland, highlighting Paleoproterozoic metasedimentary units of the Rae and other Archean cratons, as well as the location of the Rinkian belt where the Karrat Group is located (modified from [Corrigan et al., 2009](#); [Kolb et al., 2016](#)). Position of Canada with respect to Greenland is shown at 100 Ma (pre-rift) from GPlates. Baffin-Rinkian suture (BRS) from [Grocott et al. \(2023\)](#).

successions of the eastern Rae craton. One outcome of geochronological work showed that the Penrhyn and Piling groups were deposited at different times, with the Penrhyn Group being younger than 1.90 Ga, whereas the Piling Group is older than 1.90 Ga, thus their traditional correlation no longer holds ([Partin et al., 2014a](#)). Whether or not the Karrat Group correlates with either the Piling or the Penrhyn groups of the Foxe Fold belt has not been rigorously tested. Similar to the Penrhyn and Piling groups, the Karrat Group has been interpreted to represent an epicontinental rift to foreland succession ([Grocott and Pulvertaft, 1990](#); [Sanborn-Barrie et al., 2017](#)) prior to deformation by the Rinkian-Nagssugtoqidian orogen ([Henderson and Pulvertaft, 1987](#)) and the Trans-Hudson orogen ([Kirkland et al., 2017](#)). The uppermost Karrat Group (Nūkavsak Formation) was recently interpreted to be deposited in concert with the ca. 1.92 Ga Thelon orogen ([Sanborn-Barrie et al., 2017](#)), which is older than the ca. 1.9 Ga Foxe orogen that coincides with the deposition of the uppermost Piling Group (e.g., [Corrigan et al., 2009](#)). Our comprehensive geochronology and provenance analysis study here, spanning over 2600 detrital zircon grains, can clarify the Canada-Greenland connection of the sedimentary basins of the eastern Rae craton.

Previous geochronology studies of the Karrat Group have thus far been limited to U-Pb ages, with no corresponding Hf or O isotope data, with the primary goal of constraining the maximum depositional age of Karrat Group units ([Kalsbeek et al., 1998](#); [Sanborn-Barrie et al., 2017](#)). Thus, a detailed provenance study of each unit of the Karrat Group has not been conducted. The use of combined zircon U-Pb, Hf, and O isotopes can reveal the depositional history and tectonic setting of the Karrat Group, as well as the tectonic events that affected the eastern Rae craton in Greenland, beyond what is currently known or dated. This is because detrital zircon grains tend to capture a more representative crustal record than the exposed and known crustal record and can be useful in reconstructing poorly understood tectonic events (e.g., [Gehrels, 2014](#)). Provenance analysis has the potential to distinguish between the various candidates for which orogenic events in Laurentia (e.g., Rinkian, Nagssugtoqidian, Thelon) might be responsible for shedding *syn*-orogenic sediment into the Karrat basin. Here, we use zircon U-Pb, Hf, and O isotopes to determine the age, provenance, and tectonic setting of the Karrat Group. We use these data to compare with other pre- and *syn*-orogenic strata in northeast Laurentia, including the Piling and Penrhyn groups,

that were deposited on the Rae craton prior to orogenic events of the Trans-Hudson orogen that closed the Manikewan Ocean. Additionally, because very little is known about the basement rocks of the eastern Rae craton (e.g., Thrane, 2021), our combined U-Pb, Hf, and O isotopic approach also provides insight into the composition and history of Archean rocks in the study area.

2. Geological setting

The Karrat Group was deposited on Archean gneisses and orthogneisses of the Umanak gneiss (Henderson and Pulvertaft, 1987). Basement ages of the Rae craton in West Greenland (Thrane, 2021) show a bimodal age distribution from 3168 ± 12 Ma to 2662 ± 8 Ma north of the Prøven igneous complex (~ 73.5 to $\sim 76^\circ$ N) and a more uniform spread of ages from 3157 ± 3 Ma to 2706 ± 3 Ma south of the Prøven igneous complex to Maarmorilik (~ 72.5 to $\sim 70.5^\circ$ N).

2.1. Stratigraphy

The Karrat Group (Fig. 2) is a siliciclastic-carbonate-volcanic rock succession that was originally divided into two formations, the Qeqertarsuaq and Nûkavsak formations (Henderson and Pulvertaft, 1967), followed later by the additions of the Qaarsukassak, Kangilleq, and Mârmorilik formations (Henderson and Pulvertaft, 1987; Guarnieri et al., 2016; Grocott and McCaffrey,

2017). Recent mapping by the Karrat Zinc project team (e.g., Rosa et al., 2018) separates the Qeqertarsuaq Formation from the rest of the Karrat Group on the basis of a regional unconformity surface above the now-named Qeqertarsuaq complex and an additional phase of deformation within it (Guarnieri et al., 2022, 2016). Thus, the Karrat Group is defined as the Qaarsukassak, Kangilleq, Mârmorilik, and Nûkavsak formations. The stratigraphic relationships between these units are complex, and the age control on these formations is poor. The Kangilleq Formation was deposited unconformably on the Qeqertarsuaq complex or Qaarsukassak Formation (Rosa et al., 2016). The Qaarsukassak Formation infills paleotopography (paleo-valleys) created by this erosional unconformity and thus is deposited directly on basement rocks in its type area in Kangerluarsuk Fjord (Guarnieri et al., 2016), or on the Qeqertarsuaq complex. The Mârmorilik Formation is deposited directly on basement rocks, whereas the Nûkavsak Formation occurs on variable substrates (Kangilleq, Qaarsukassak, Mârmorilik, and basement rocks). True stratigraphic thickness is not known, but the entire succession of the Karrat Group is thought to be > 5 km thick (Henderson and Pulvertaft, 1987).

The Qeqertarsuaq complex varies considerably both in lithology (semipelitic to pelitic schist, quartzite, quartzitic schist, marble, hornblende schist, and amphibolite) and in structural thickness (140–3000 m), and was metamorphosed to amphibolite facies conditions (Henderson and Pulvertaft, 1987). The Qaarsukassak Formation is relatively thin and variable in stratigraphic thick-

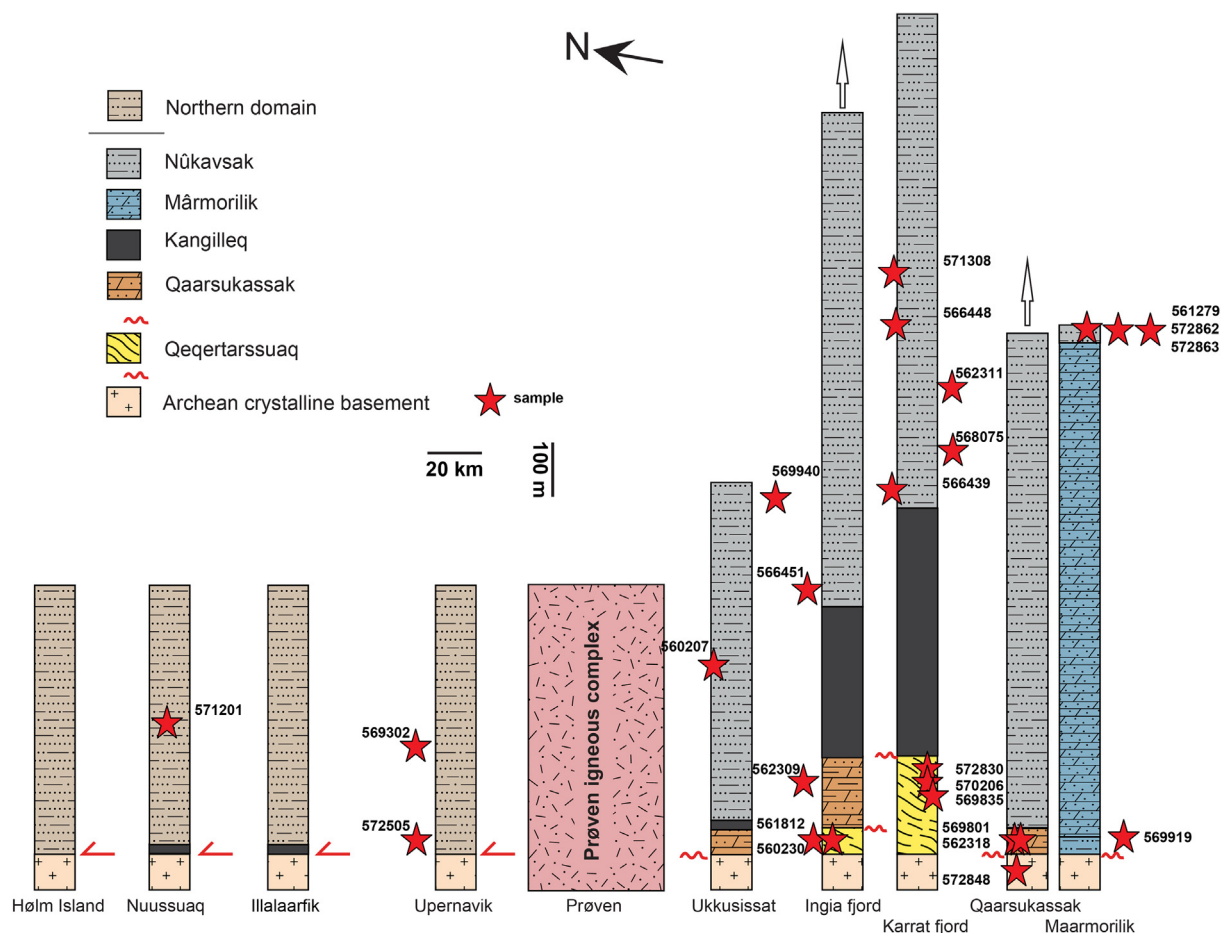


Fig. 2. Stratigraphy of supracrustal rocks, including the Karrat Group (Qaarsukassak, Kangilleq, Mârmorilik, Nûkavsak formations), across coastal West Greenland from Maarmorilik (south) to Hølm Ø (north). Stratigraphic thickness for Karrat Group units estimated from field observations; tectonostratigraphic thickness highly uncertain for the northern domain metasedimentary rocks (Karrat Group, sensu lato). The Prøven igneous complex is the geological boundary between the Karrat Group and the northern domain metasedimentary rocks. Estimated stratigraphic position of samples is shown.

ness, consisting of a fining-upward sequence of quartzite, metasediment and metamudstone, and graphitic quartzite, overlain by calcitic metacarbonate rocks, which are in turn overlain by quartzite and marble (Guarnieri et al., 2016). The Qaarsukassak Formation is bounded by the Nûkavsak Formation and Archean basement rocks, on which a depositional contact is preserved (Partin, 2018). Thickness variations along strike suggest that it was deposited into pre-existing topographical lows on Archean rocks within a fluvial to shallow marine environment associated with a marine transgression.

The Marmorilik Formation is dominantly composed of calcitic and dolomitic metacarbonate rocks, with a basal sequence dominated by siliciclastic rocks, including quartzite, conglomerate, and calcareous metasediment (Garde, 1978; Rosa et al., 2017). Symmetrical ripple marks in the basal metasediment unit of the Marmorilik Formation suggest it was deposited in a shallow marine environment; the presence of stromatolites in the dolomitic marble suggests the shallow marine environment (<100 m water depth) continued throughout the carbonate succession (Partin, 2018). The Marmorilik Formation is separated from outcrops of the Qaarsukassak Formation by a basement topographic high (Fig. 2), suggesting that these two formations were deposited in separate sub-basins (Grocott and Pulvertaft, 1990). It is not known if they were deposited coevally. The Marmorilik Formation has a structural thickness of ~1600 m and is metamorphosed to lower amphibolite facies (Garde, 1978; Grocott and McCaffrey, 2017; Pedersen, 1980). The uppermost Marmorilik Formation “semipelite” unit is tentatively correlative with Nûkavsak Formation; however, this is uncertain because the Marmorilik and Nûkavsak formations are not in contact with each other (Henderson and Pulvertaft, 1987). We test this correlation in this study.

The Kangilleq Formation is a package of alkaline to transitional basaltic mafic metavolcanic rocks that include pillow lava, tuff, and volcanoclastic rocks, which is stratigraphically above the Qaarsukassak Formation (Rosa et al., 2017). The Kangilleq Formation has a structural thickness ranging from ~10 to 850 m and is interbedded with the basal unit of the Nûkavsak Formation, suggesting a conformable relationship between these two units (Rosa et al., 2017). Thus, our geochronological results from the Nûkavsak Formation provide insight into the absolute age of Kangilleq volcanism on the eastern Rae craton.

The Nûkavsak Formation is primarily composed of metagreywacke and pelitic schist interpreted to represent turbidite, or flysch-type, deposits and is at least 4000 m thick (Henderson and Pulvertaft, 1987). Despite deformation, including foliation, thrusts, and chevron-style folds in some areas, many primary sedimentary structures are preserved, including normal grading, flute casts, scour structures, flame structures, parallel cross-bedding, convolute lamination, and climbing ripples (Grocott and Vissers, 1984; Henderson and Pulvertaft, 1987). Henderson and Pulvertaft (1987) interpreted the Nûkavsak Formation to represent flysch deposits in a foreland basin setting, whereas Grocott and Pulvertaft (1990) did not favor a foreland model due to a lack of slumps, seismoturbidites, and/or lateral facies changes. More recently, Grocott and McCaffrey (2017) argued for foreland basin for the upper Nûkavsak Formation, and a post-rift sequence for the lower Nûkavsak Formation. Previous work has suggested that the Nûkavsak Formation broadly correlates with other pre-to-syn orogenic siliciclastic units on the Rae craton (e.g., Jackson and Taylor, 1972), which we address in our study.

Supracrustal rocks attributed to the Karrat Group crop out from the Marmorilik and Aqpat areas in the south (~70°50'N) to the Red Head locality in the north (~75°). Reconnaissance geological mapping revealed differences between the supracrustal rocks assigned to the Karrat Group north of the Prøven igneous complex (~72°10'N to 73°05'N) and those that occur south of the Prøven

igneous complex (Rosa et al., 2018). The map compilation by Escher and Watt (1976) notes that the “metagreywacke” map unit has a “gneissic aspect north of 72°30'N”. Thus, the differences were initially thought to reflect differences in metamorphic grade, but field observations show that the lithofacies and stratigraphy differ greatly between the northern supracrustal rocks and the southern supracrustal rocks (Marmorilik, Nûgâtsiaq, and Pangnertôq 1:100 k map sheets; Henderson and Pulvertaft, 1987; updated recently by Guarnieri et al., 2022). We explore this difference between supracrustal rocks north and south of the Prøven igneous complex in our study.

Deformation by orogenic events resulted in at least three deformation events (Rosa et al., 2018) that are characterized by compressional tectonics, including both thin- and thick-skinned thrust faults. The first event affecting the Karrat Group is defined by east to southeast tectonic transport and a thin-skinned fold-and-thrust belt, attributed to the Rinkian orogen. The second and third events are defined by north-northeast to northeast and southeast tectonic transport, respectively, and are attributed to deformation associated with the Nagssugtoqidian orogen, or possibly as further deformation associated with the Rinkian orogen (Guarnieri and Baker, 2022; Rosa et al., 2018). On the other hand, Grocott and McCaffrey (2017) interpret the structural evolution to include an eastward tectonic transport followed by northwestward tectonic transport in the “Karrat Fjord thrust system” during some combination of the Rinkian and Nagssugtoqidian orogens, or possibly from an east–west orogenic event related to the convergence and collision of Baffin Island and West Greenland (Grocott et al., 2023). Additionally, a top-to-the-northwest ductile shear zone at Tussaak (Rosa et al., 2018), first identified by Escher and Stecher (1978), that occurs north of the Prøven igneous complex could be important for understanding the differences between the northern and southern supracrustal rocks and/or the origin of the Prøven igneous complex.

2.2. Existing age constraints on the Karrat Group

Kalsbeek et al. (1998) produced the first U-Pb detrital zircon ages for the Nûkavsak Formation. They found a dominant population of ca. 2.1–1.95 Ga grains, which, guided by whole-rock Sm-Nd data, they tentatively interpreted as being derived from a magmatic arc, which they inferred to be either no longer preserved, under inland ice cover, or otherwise unknown. A metagreywacke sample with a youngest detrital zircon of 1969 ± 9 Ma showed ca. 2169–2476 Ma and ca. 2532–3040 Ma zircon populations, the older of which were assumed to be derived from local basement rocks. More recent detrital zircon U-Pb geochronology (Sanborn-Barrie et al., 2017) showed youngest detrital zircon for the Nûkavsak Formation (on Karrat Island) is 1953 ± 31 Ma with primary age peaks between ca. 2.00 and 1.97 Ga and secondary age peaks between ca. 2.7 and 2.5 Ga. The youngest detrital zircon for a psammite from the northern supracrustal rocks from the northern edge of the belt on Holm Island is 1905 ± 20 Ma.

The Prøven igneous complex covers an area of ~4500 km² in the Upernavik region and is composed of various igneous phases that were emplaced over 30 Myr from ca. 1.87 to 1.90 Ga. These phases include charnockite (1869 ± 20 Ma; Thrane et al., 2005), quartz diorite (1876 ± 4 Ma), quartz monzonite (1893 ± 9 Ma), and granodiorite (1900 ± 4 Ma) phases (Sanborn-Barrie et al., 2017). The Prøven igneous complex intrudes Archean orthogneisses plus the supracrustal rocks of the Karrat Group and contains inclusions of metasedimentary rocks (Thrane et al., 2005). The Prøven igneous complex was originally interpreted to have resulted from collision-induced delamination during the Rinkian orogen (Thrane et al., 2005), but has been recently reinterpreted as I-type granites that formed in an upper-plate, continental magmatic

arc setting, which has led to a new tectonic model (Grocott et al., 2023). Older phases of the Prøven igneous complex overlap in age with the ca. 1.899–1.886 Ga monzogranite–granodiorite Qikiqtarjuaq plutonic suite (Rayner et al., 2012; Rayner, 2017) on the Cumberland Peninsula of eastern Baffin Island. The Qikiqtarjuaq plutonic suite intrudes Archean basement rocks of the Rae craton and the Hoare Bay Group and crosses the Baffin suture that stitches the Rae craton and Meta Incognita microcontinent (Rayner, 2017).

Low Th/U zircon rims dated at 1840 ± 7 Ma provide a constraint of high-temperature metamorphism in the northern Karrat Group (Sanborn-Barrie et al., 2017). Two samples of the Prøven igneous complex also contain low Th/U zircon rims at 1836 ± 17 Ma and 1829 ± 6 Ma (Sanborn-Barrie et al., 2017). These zircon rim ages show that regional high-temperature (granulite facies) metamorphism of the Prøven igneous complex and the supracrustal rocks found north of the Prøven igneous complex occurred at similar times. Additionally, U-Pb ages on apatite (1826 ± 9 Ma formed at ≥ 485 °C) and titanite (1768 ± 8 Ma formed at ≤ 452 °C) from the Kangilleq Formation are interpreted to represent metamorphic mineral growth during the terminal collision of the Rae craton with the Superior craton during the Trans-Hudson orogen and the younger Nagssugtoqidian orogen, respectively (Kirkland et al., 2017). Further, Sm-Nd, Pb-Pb, and Lu-Hf isochron-ages from the Prøven igneous complex show ca. 1840–1800 Ma model ages (Thrane et al. 2005). Ca. 1795–1782 Ma cooling ages from Ar-Ar (hornblende) are interpreted to represent cooling to greenschist facies (Sidgren et al., 2006). Thus, dating of metamorphic mineral phases (zircon rims, titanite, apatite) provides an age for peak metamorphism at ca. 1.83 Ga for the southern domain Karrat Group and ca. 1.84 Ga for the northern domain Karrat Group. From this spectrum of ages, it is reasonable to assign peak regional metamorphism of the Karrat Group to ca. 1.83–1.80 Ga with cooling ca. 1.79–1.77 Ga, which represents a time of indentation tectonics in northeast Laurentia, between the Superior craton and Churchill province (Corrigan et al., 2021).

2.3. Paleoproterozoic orogenic events affecting the Rae craton in Canada and west Greenland

The Rinkian orogen was originally defined based on its structural style, including nappes with superimposed domes, and the presence of the Karrat Group cover sequence, spanning a ~600 km-wide collisional zone from the Disko Bugt area to Red Head (Pulvertaft, 1973; Escher and Watt, 1976; Grocott and Pulvertaft, 1990; Connelly et al., 2006). The Rae and North Atlantic cratons in West Greenland are separated by the Nagssugtoqidian orogen with a suture in the Disko Bugt region that likely represented a south-dipping subduction zone (Connelly et al., 2006; Connelly and Thrane, 2005; Garde and Hollis, 2010; Kolb, 2014; van Gool et al., 2002). The collision of the Rae and North Atlantic cratons, the collision of the Rae craton and the Aassiat domain (St-Onge et al., 2009), as well as the terminal collision in the Trans-Hudson orogen of the Superior craton with the Rae craton and its constituents are thought to be responsible for the compressional tectonic structures and metamorphism in the Karrat Group. Recently, a ca. 1.81 Ga suture has been proposed to exist between the Rae craton of Baffin Island and the Rae craton of West Greenland, called the Baffin-Rinkian suture, representing a former subduction zone of oceanic lithosphere between 1.95 Ga and 1.82 Ga (Grocott et al., 2023).

3. Materials and methods

3.1. Samples

Samples were collected from outcrop during field expeditions from 2015 to 2017 (Fig. 3) in West Greenland. Zircon grains were separated from eight samples and analyzed by the laser-ablation split stream inductively coupled plasma mass spectrometry (LASS ICP-MS) technique for zircon U-Pb and Hf isotopes, as well as O isotopes by ion microprobe: four metasandstones (arkose to litharenite) from the Nûkavsak Formation (571308, 566448, 566439, 566451), one metasandstone (subarkose) from the Qeqqartarsuaq Formation (572830) and one metasandstone (arkose) from north of the Prøven igneous complex (572505), and two metasandstones (litharenite) from upper Marmorilik Formation (572862, 572883). The same techniques were used to analyze two Archean orthogneiss samples (572806, 572848) to further elucidate local basement ages and their Lu-Hf and O isotope systematics. Sample photos are shown in Supplementary Data (Fig. S1). Additional samples were analyzed for detrital zircon U-Pb analysis by single-instrument by LA-ICP-MS for this study: four samples from the Qeqqartarsuaq complex (560230, 561812, 570206, 569835), eight samples from the Qaarsukassak Formation (569801, 562318, 562309, 568083, 569938, 560205, 569901, 568050), four samples from the Nûkavsak Formation, (560207, 562311, 569940, 568075), two samples from the Marmorilik Formation (561279, 569919), and two metasedimentary samples from north of the Prøven igneous complex (571201, 571239). The U-Pb data for samples 571201, 571239, 560205, and 569801 generated at Geological Survey of Denmark and Greenland laboratories were recently included in two publications (Grocott et al., 2023; Guarnieri et al., 2023), however those data are integrated here to provide an in-depth analysis of variations in provenance within and surrounding the Karrat stratigraphy. Overall, twenty-three detrital samples were analyzed from different formations within the Karrat Group and five samples from within the Qeqqartarsuaq complex.

3.2. Analytical methods

3.2.1. Mineral separation

Samples collected in 2015–2017 during field work in West Greenland (572862, 572883, 572806, 572848, 572505, 572830, 571308) were processed at the University of Saskatchewan for later analysis by LASS ICP-MS and ion microprobe at the University of Alberta. Samples were crushed using a combination of the Terminator Jaw Crusher and a SELFRAG (at the Saskatchewan Research Council). The samples were further processed using a DMP-100 Disc Mill to achieve a uniform grain size distribution then sieved to collect a grain size distribution between 90 μm to 300 μm prior to water density separation. Samples were dried prior to density separation that used methylene iodide (3.32 g/cm^3) at the Saskatchewan Research Council and the University of Saskatchewan. A Frantz Magnetic Separator (Model L-1) with a 20-degree forward slope, voltage at 29.4 V, and current at 0.45 A was used to separate magnetic and non-magnetic mineral fractions. To decrease bias, a representative zircon grain population was picked, with respect to morphology, color, magnetic fractions, and grain size. All other samples collected in 2015–2017 were processed at the Geological Survey of Denmark and Greenland using similar standard zircon separation techniques.

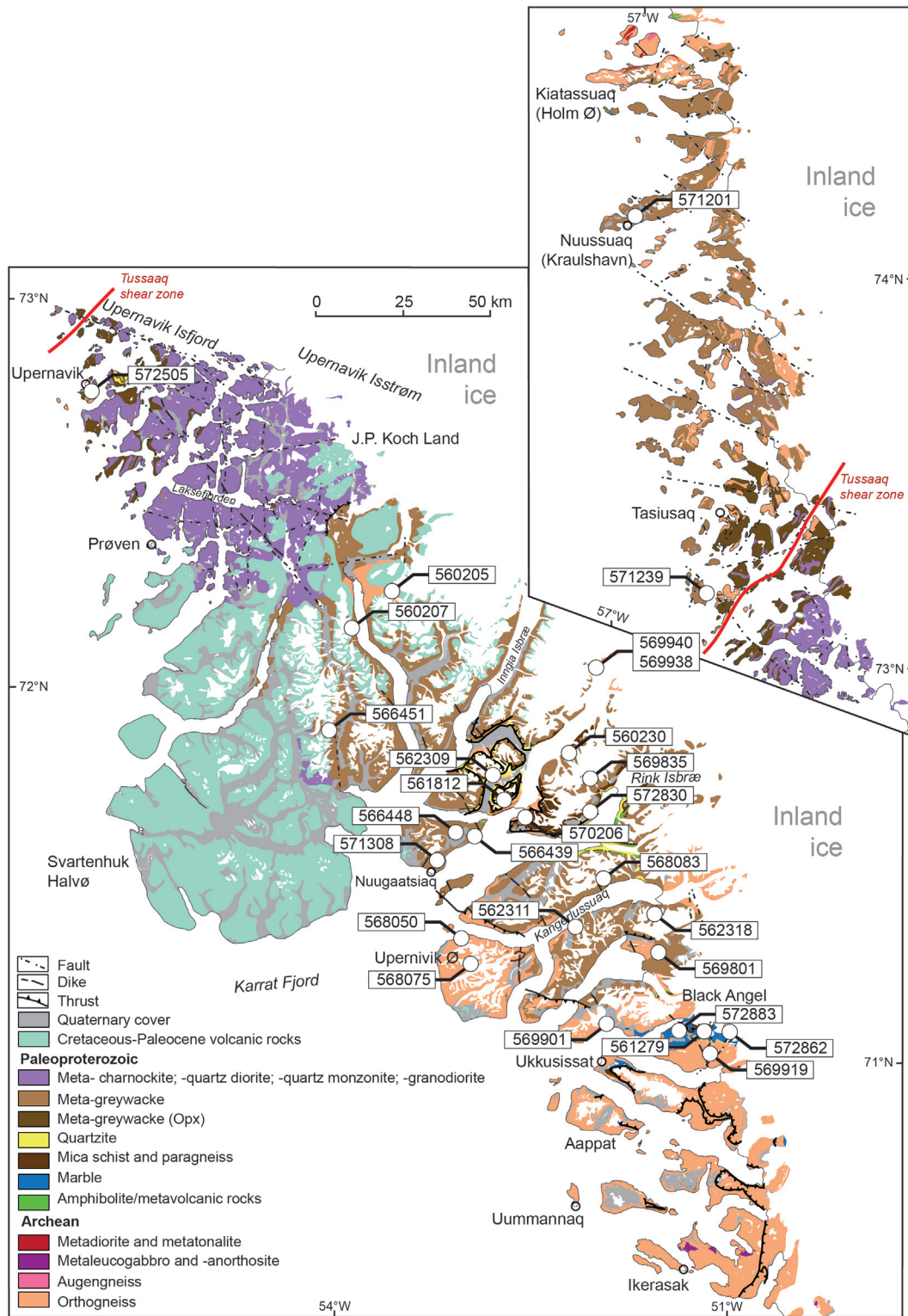


Fig. 3. Geological map of the study area (after Kolb et al., 2016). White circles denote detrital zircon U-Pb geochronology samples and U-Pb, Hf, O samples from the Karrat Group analyzed in this study.

3.2.2. Backscattered electron and cathodoluminescence imaging

At the Canadian Centre for Isotopic Microanalysis (University of Alberta), polished zircon mid-sections of unknown zircon grains and zircon reference materials were exposed using diamond grits and coated with 10 nm of high-purity Au. Zircon grains were imaged by backscattered electron (BSE) and

cathodoluminescence (CL) using a Zeiss EVO MA15 scanning electron microscope, equipped with a high-sensitivity, broadband CL detector and a BSE detector. Beam conditions were 15 kV and 3–53nA sample current. Zircon spot targets were chosen based on the BSE and CL images, avoiding inclusions or metamict zones.

3.2.3. U-Pb geochronology and Hf isotopes

The LASS ICP-MS technique at the University of Alberta, which uses two independent mass spectrometers for the collection of multiple isotope systems during a single ablation (Fisher et al., 2014), was employed for the determination of the U-Pb age and Hf isotope composition of zircon grains in ten samples. A single collector Element2 XR ICP-MS was used for the U-Pb isotope system and a Thermo Neptune Plus multicollector (MC) ICP-MS was used for the Lu-Hf isotope system. The laser beam diameter was 33 μm , with an 8 Hz repetition rate and producing a laser fluence of 3 J/cm². Both samples and standards were ablated for 40 s at each spot to measure the ²⁰⁶Pb/²³⁸U, ²⁰⁷Pb/²³⁵U, ²⁰⁶Pb/²⁰⁷Pb, ¹⁷⁶Lu/¹⁷⁷Hf, and ¹⁷⁶Hf/¹⁷⁷Hf ratios. Data were processed using Iolite 3.X, via a custom-made data reduction scheme (Fisher et al., 2017). LH94-15 was used for the primary standard for the U-Pb isotope system with Plešovice and 91500 as the secondary standards. For the Lu-Hf system, Plešovice was the primary standard with FC-1 as the secondary standard. MUN-1 and MUN-3 synthetic zircon standards were used to correct for Yb interferences. A summary of zircon reference material data for the LASS ICP-MS analysis sessions is shown in [Supplementary Data \(Fig. S2\)](#).

An additional 20 samples were analyzed for detrital zircon U-Pb geochronology at the Geological Survey of Denmark and Greenland in Copenhagen using a Thermo-Scientific ELEMENT2 Sector Field ICP-MS coupled to a NWR UP213 laser ablation unit equipped with a frequency-quintupled solid state Nd:YAG laser. Methods followed those of Frei and Gerdes (2009) and are summarized in Thrane (2021).

Combining datasets from the two methods provides interlaboratory confirmation of age data, strengthening confidence in replication of geochronological results. All U-Pb detrital zircon ages were filtered to include those with $\leq \pm 10\%$ discordance and are illustrated using a combined frequency histogram with probability density curves (Fig. 4). The maximum depositional age calculation (Table 1) was determined via a weighted average of the three youngest detrital grains (Supplementary Data). Filtering criteria (discordance $\pm 10\%$, Th/U > 0.1 (Hoskin and Schaltegger, 2003), error correlation < 1) in addition to a visual inspection of zircon quality and considerations of metamorphic age were used to determine the youngest detrital grains. For the higher metamorphic grade northern domain metasedimentary samples, a higher Th/U cutoff of 0.4 (Yakymchuk et al., 2018) was used.

3.2.4. Oxygen isotopes

A Cameca IMS 1280 multicollector ion microprobe at the University of Alberta was used to analyze the oxygen isotopes (¹⁸O/¹⁶O) of individual zircon spots. Oxygen isotope analysis was conducted prior to LASS analysis; thus, there were far more oxygen isotope analyses conducted (n = 845) than are reported here (n = 335), as those presented are associated with concordant U-Pb data in the same zircon zone. On the ion microprobe, a ¹³³Cs⁺ primary beam with 20 keV energy impact and current of 1.5–2.0 nA was used. Before the analysis the $\sim 12\ \mu\text{m}$ probe was rastered for 45 s; during analysis, a rectangular area measuring $\sim 15 \times 18\ \mu\text{m}$ and $\sim 2\ \mu\text{m}$ deep was created. For charge compensation, a normal incidence electron gun was used and negative secondary ions were extracted through 10 kV into the secondary column. Faraday cups L2 (¹⁶O⁻) and H2 (¹⁸O⁻) at mass resolutions (m/ Δ m at 10 %) of 1950 and 2250 detected separated oxygen ions simultaneously. The instrumental mass fractionation (IMF) was monitored by repeated analysis of two reference materials (RM S0081 = UAMT1 with $\delta^{18}\text{O}_{\text{VSMOW}} = +4.87\ \text{‰}$; R. Stern, unpublished laser fluorination data, University of Oregon) after four unknowns and TEM2 ($\delta^{18}\text{O}_{\text{VSMOW}} = 8.20\ \text{‰}$; Black et al., 2004) after every 12 unknowns. The primary reference material resulted in standard deviations of 0.10–0.13 ‰ per session with the IMF ranging from

0.1–1.4 ‰. The within-spot counting statistics, between spot geometric effects, and correction for IMF gave uncertainties of ± 0.25 at a 95 % confidence for $\delta^{18}\text{O}_{\text{VSMOW}}$. The secondary reference material (TEM2) was further analyzed on multiple spots and multiple grains, resulting in mean values for $\delta^{18}\text{O}_{\text{VSMOW}} = +8.23 \pm 0.04\ \text{‰}$ (MSWD=0.94; n = 31), $+8.20 \pm 0.06\ \text{‰}$ (MSWD=1.2; n = 22, 1 reject), $+8.20 \pm 0.05\ \text{‰}$ (MSWD=0.85; n = 20), and $+8.29 \pm 0.07\ \text{‰}$ (MSWD=0.43; n = 8).

3.3. Database methods and paleogeographic reconstruction

Potential sources were determined by identifying clusters of detrital zircon peak ages from our samples, matching them to published U-Pb crystallization ages, as well as Sm-Nd and Lu-Hf tracer isotope data that were retrieved from the DateView database (Eglington, 2004), and superimposing these ages on the Rae craton and nearby terranes and cratons using GPlates for visualization of provenance. GPlates and arcGIS were used in tandem to visually represent potential provenance for the Karrat Group on craton maps that represent paleogeographic reconstructions at approximately 2.6 Ga, 2.0 Ga, 1.95 Ga, and 1.90 Ga, representing the maximum depositional ages of units. Literature data typically contains ϵNd data (and less commonly ϵHf values), thus the Terrestrial Nd-Hf isotope Array (Vervoort et al., 2011) was used to convert ϵNd values into ϵHf values to compare the isotopic systems to each other using $\epsilon\text{Hf} = 1.55^* \epsilon\text{Nd} + 1.21$. Any whole-rock ϵNd values from the database that have been converted into ϵHf are denoted with an asterisk (ϵHf^*).

4. Results

4.1. U-Pb geochronology

Data for 28 detrital samples are presented here to constrain the provenance, maximum depositional age, and detrital age frequency distribution of the Qeqertarsuaq complex, Karrat Group, and metasedimentary units north of the Prøven igneous complex (Fig. 2). All U-Pb detrital zircon ages are shown in a combined frequency histogram with probability density curves (Fig. 4, Supplementary Data Fig. S3). A large number of zircon analyses from each unit allows for rigorous testing of age and provenance (Marmorilik, n = 393; Nükavsak, n = 665; Qaarsukassak, n = 797; northern domain metasedimentary rocks, n = 411; Qeqertarsuaq complex, n = 394). Two Archean orthogneiss samples occur either beneath the Qaarsukassak Formation (572848/ S4858) or structurally above the Nükavsak Formation (572806/ S4856). A summary of detrital U-Pb geochronological results including the maximum depositional age and dominant and subdominant age peaks for each sample are listed in Table 1. Full data results are listed in [Supplementary Data and Table S1](#).

4.2. Lu-Hf isotopic data

Zircon from a total of eight Karrat metasedimentary rock samples were analyzed for Lu-Hf isotope data (n = 654 spots) via LASS and are plotted against U-Pb crystallization ages (Fig. 5). The results of the Lu-Hf analysis of the six samples from the Karrat Group, one sample from the Qeqertarsuaq complex, and one sample from the northern domain metasedimentary rocks are listed in [Supplementary Data Table S1](#). The depleted mantle line is illustrated by using the ¹⁷⁶Lu decay constant of $1.867 \times 10^{-11}\ \text{yr}^{-1}$ (Söderlund et al., 2004) and a ¹⁷⁶Lu/¹⁷⁷Hf value of 0.0338 with the present day ¹⁷⁶Hf/¹⁷⁷Hf value of 0.28325 (Griffin et al., 2002). The results for ϵHf values are from zircon grains within $\pm 10\%$ discordance in their U-Pb age (Fig. 5).

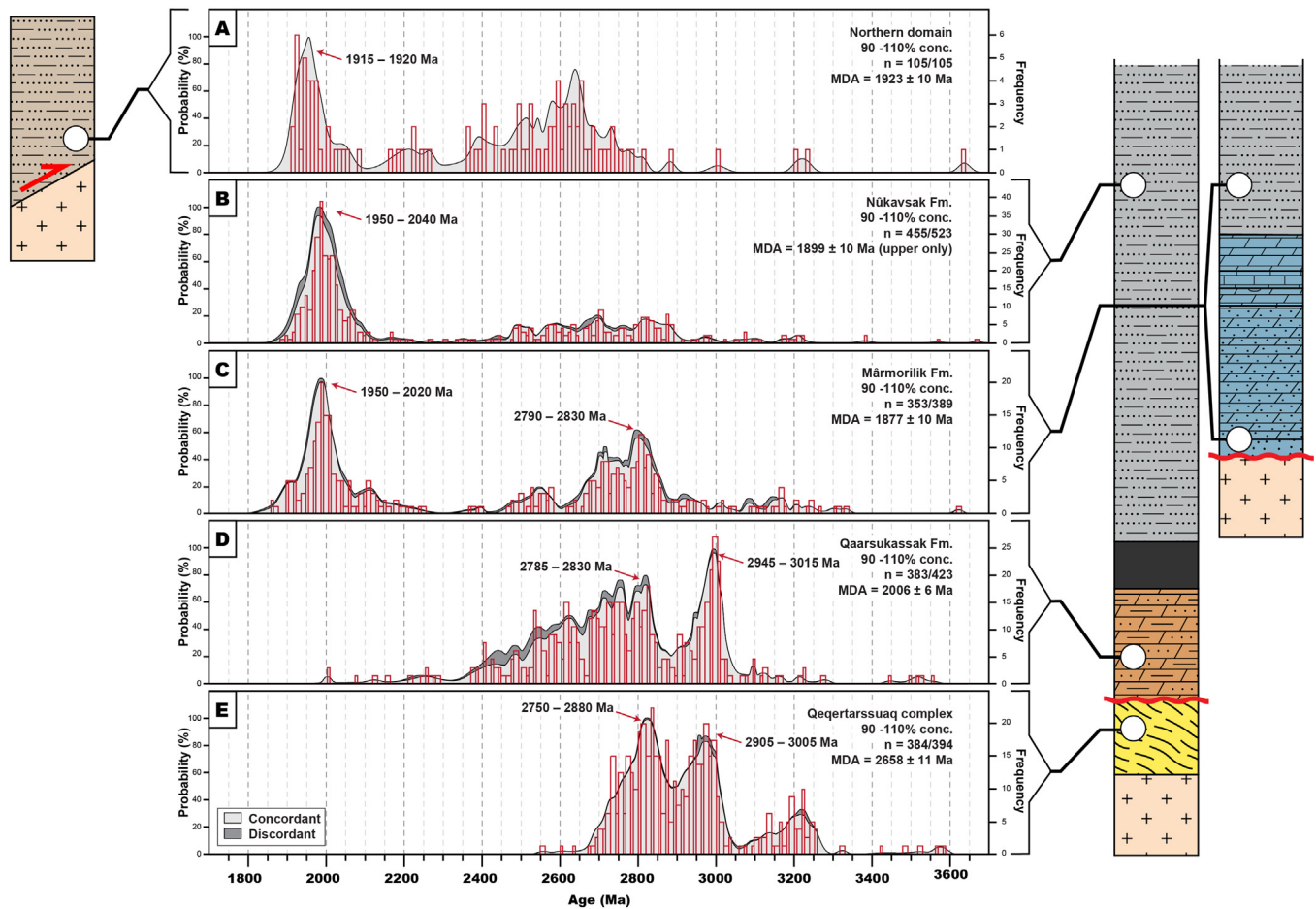


Fig. 4. Combined frequency histogram with normalized probability density curves of detrital zircon U-Pb geochronology results: Qeqertarsuaq complex, Karrat Group (Qaarsukassak, Mârmorilik, Nûkavsak formations) and northern domain Karrat Group with relative stratigraphic position indicated. Both concordant (90–100 % concordance, light grey) and discordant (dark grey) zircon U-Pb ages are plotted; the number of concordant grains is listed along with the total number of grains. The maximum depositional age (MDA) listed for each unit is a weighted mean of the three youngest detrital zircon grains. All the Nûkavsak samples are combined here, whereas [Table 1](#) details the MDA of each stratigraphic level.

4.2.1. Qeqertarsuaq complex

A subarkose from the Qeqertarsuaq complex (572830/S4857) shows ϵ_{Hf} values ranging from -8.0 to $+9.3$. All U-Pb grain ages are Archean (2559–3584 Ma). The majority of the ϵ_{Hf} values are positive (68 %) and the remainder are negative (32 %). The largest population of positive ϵ_{Hf} values are associated with grain ages between ca. 2870 and 2800 Ma.

4.2.2. Nûkavsak Formation

Four metasediments (arkose to lithic arkose to litharenite) samples from the Nûkavsak Formation (566451/S4855, 566448/S4854, 566439/S4853, 571308/S489) have ϵ_{Hf} values ($n = 245$) that range from -15.1 to $+11.2$. Within this range, 72 % of the ϵ_{Hf} values are positive ($n = 177$) and 28 % of the values are negative ($n = 68$). The largest cluster of positive ϵ_{Hf} values correspond to grains with U-Pb ages between ca. 2150 and 1950 Ma. The most positive ϵ_{Hf} values in the Nûkavsak dataset correspond to grain ages of ca. 2200 and 2100 Ma, whereas the most negative ϵ_{Hf} values correspond to grain ages of ca. 2200 Ma.

4.2.3. Mârmorilik formation

Two litharenites from the upper Mârmorilik Formation (572883/S4859, 572862/S4893) show ϵ_{Hf} values ($n = 157$) that range from -17.2 to $+14.9$. Within this range, 73 % of the ϵ_{Hf} values are positive ($n = 114$) and the remainder of the ϵ_{Hf} values are neg-

ative ($n = 43$). Similar to the Nûkavsak Formation samples, the largest cluster of positive ϵ_{Hf} values correspond to grains with U-Pb ages between ca. 2100 and 1950 Ma. The most positive ϵ_{Hf} values in the Mârmorilik dataset correspond to grain ages of ca. 2250 and 2150 Ma, whereas the most negative ϵ_{Hf} values correspond to grain ages of ca. 2250 and 1950 Ma.

4.2.4. Northern domain metasedimentary rocks

An arkose from the northern domain metasedimentary rocks (572505/S4892) shows ϵ_{Hf} values ($n = 77$) ranging from -24.5 to $+1.7$. Most ϵ_{Hf} values (97 %) are negative ($n = 75$) and the remainder of the ϵ_{Hf} values are positive. Positive ϵ_{Hf} values are associated with grain ages of ca. 2800 Ma, whereas the negative ϵ_{Hf} values are associated with grain ages from ca. 1970 to 1850 Ma. The Paleoproterozoic grain ages are associated with Pb-loss ([Supplementary Data Fig. S4](#)) and thus are not shown on [Fig. 5](#).

4.2.5. Igneous samples

Two Archean gneissic to granitic igneous samples (572806/S4856, 572848/S4858) with ages of 2772.2 ± 2.7 Ma and 2805.1 ± 1.5 Ma, respectively, show ϵ_{Hf} values between -13 and $+5$ for sample 572806 and -6 and $+5$ for sample 572848 ([Supplementary Data Fig. S4](#)).

Table 1

Summary of detrital U–Pb geochronological data including the maximum depositional age and dominant and subdominant age peaks. Age in bold represents the maximum depositional age (weighted mean of youngest three detrital grains) for the unit.

Sample ID	Unit name	Maximum depositional age	Dominant age peaks (Ma)	Subdominant age peaks (Ma)
572830/S4857	Qeqertarsuaq	2660 ± 7.6 Ma	2800–2865 Ma	2960–2990, 3200 Ma
560230	Qeqertarsuaq	2658 ± 11 Ma	2740–2855 Ma	3110, 3180 Ma
561812	Qeqertarsuaq	2695 ± 5.9 Ma	2716–2790 Ma	2850–3013, 3094–3240, 3513–3530 Ma
570206	Qeqertarsuaq	2819 ± 12 Ma	2940–3016 Ma	3088–3097, 3132–3159 Ma
569835	Qeqertarsuaq	2749 ± 16 Ma	2894–3003 Ma	3160–3262 Ma
569801	Qaarsukassak (base)	2006 ± 6.4 Ma	2710–2835 Ma	2939–2998, 3089–3100, 3009–3016, 3156–3165 Ma
562318	Qaarsukassak	2697 ± 12 Ma	2700–2736 Ma	2780, 2838, 2934 Ma
562309	Qaarsukassak	2771 ± 15	2921–3014 Ma	
568083	Qaarsukassak	2604 ± 6.8 Ma	2546–2561, 2869–2932 Ma	
569938	Qaarsukassak	2193 ± 12 Ma	2612–2797 Ma	
560205	Qaarsukassak	2596 ± 16 Ma	2775–2843 Ma	
569901	Qaarsukassak	2121 ± 12 Ma	2645–2468 Ma	
568050	Qaarsukassak	2491 ± 19 Ma	Metamorphic age peak	2089–2093, 2623–2847 Ma
566451/S4855	Nûkavsak (lower)	1978 ± 7.0 Ma	1955–2048 Ma	2174 Ma, 2617–2761 Ma
566439/S4853	Nûkavsak (lower)	1981 ± 6.0 Ma	1971–2030 Ma	2560, 2620, 2880, 3220 Ma
566448/S4854	Nûkavsak (middle-upper)	1969 ± 6.7 Ma	1965–2024 Ma	2474–2535, 2555–2823 Ma
571308/S4891	Nûkavsak (middle-upper)	1956 ± 9.1 Ma	2762–2891, 1964–2041 Ma	2089–2114, 2488–2506, 2687, 3102, 3159–3225 Ma
560207	Nûkavsak (middle)	1929 ± 8.9 Ma	1959–2025 Ma	2355, 2630 Ma
562311	Nûkavsak (middle)	1953 ± 11 Ma	1960–2031 Ma	2085, 2570, 2688 Ma
569940	Nûkavsak (upper)	1899 ± 10 Ma	1913–2008 Ma	2542–2613, 2665–2715, 2872–2884 Ma
568075	Nûkavsak (upper)	1945 ± 8 Ma	1933–2031 Ma	2672–2714, 2856–2877 Ma
572862/S4893	Mârmorilik (upper)	1902 ± 10 Ma	1952–2021 Ma	2536–2585, 2694–2758, 2784–2855 Ma
572883/S4859	Mârmorilik (upper)	1877 ± 9.5 Ma	1959–2032 Ma	1906, 2528, 2775 Ma
561279	Mârmorilik (upper)	1903 ± 7.3 Ma	1952–2008 Ma	2658–2747, 2489–2549 Ma
569919	Mârmorilik (base)	2648 ± 6.9 Ma	2700–2851 Ma	3074–3184 Ma
572505/S4892	Northern domain metasedimentary rocks	2596 ± 8.9 Ma	Apparent ages from 1900–1980 Ma	2720–2820 Ma
571201	Northern domain metasedimentary rocks	1923 ± 10 Ma	1920–1979 Ma	2188–2228, 2497–2666 Ma
571239	Northern domain metasedimentary rocks	2438 ± 1.8 Ma	Metamorphic age peak	2490, 2630 Ma

4.3. Oxygen isotopes

Detrital zircon grains with concordant U–Pb ages from five samples of the Nûkavsak, Mârmorilik formations, and Qeqertarsuaq complex (572883/S4859, 566448/S4854, 566439/S4853, 566451/S4855, 572830/S4857) in addition to two granitic basement samples (572806/S4856, 572848/S4858) were analyzed for oxygen isotopes ($n = 335$; Fig. 6).

The Nûkavsak Formation contains zircon $\delta^{18}\text{O}$ values ($n = 135$) that range between 5.2 ‰ and 11.4 ‰. Within this range there are sixty-four $\delta^{18}\text{O}$ values < 6.5 ‰, a benchmark typically regarded as reflecting a “juvenile” origin (e.g., Hawkesworth and Kemp, 2006). In general, the $\delta^{18}\text{O}$ values in Nûkavsak Formation zircon increase from the Archean to the Paleoproterozoic. Between ca. 3.67 and 2.45 Ga, the $\delta^{18}\text{O}$ values range between 5.6 ‰ and 8.7 ‰. The Paleoproterozoic ages that are between ca. 2.3 and 1.95 Ga have $\delta^{18}\text{O}$ values between 5.2 ‰ and 11.4 ‰. The upper Mârmorilik Formation contains $\delta^{18}\text{O}$ values ($n = 64$) that range between 5.1 ‰ and 9.3 ‰ with forty-seven $\delta^{18}\text{O}$ values < 6.5 ‰. The zircon $\delta^{18}\text{O}$ values in the upper Mârmorilik Formation also show increasing values from Archean to Paleoproterozoic grains. Between ca. 3.3 and 2.45 Ga, many grains ($n = 25$) have $\delta^{18}\text{O}$ values that are < 6.5 ‰, with a single evolved $\delta^{18}\text{O}$ value of 8.1 ‰. Between ca. 2.37 to 1.90 Ga there are twenty-two $\delta^{18}\text{O}$ values that are < 6.5 ‰ with sixteen $\delta^{18}\text{O}$ values that are > 6.5 ‰. The Qeqertarsuaq complex contains $\delta^{18}\text{O}$ values ($n = 103$) that range from 5.0 ‰ to 7.2 ‰, the majority of which are < 6.5 ‰. Granite sample

572848 yields $\delta^{18}\text{O}$ values ($n = 18$) between 5.0 ‰ and 7.8 ‰, with most of the $\delta^{18}\text{O}$ values < 6.5 ‰ (Supplementary Data Fig. S4, Table S2). Granite sample 572806 yields $\delta^{18}\text{O}$ values ($n = 15$) between 5.2 ‰ and 8.5 ‰, all of which are < 6.5 ‰ except for the 8.5 ‰ value (Supplementary Data Fig. S4, Table S2).

Overall, the detrital zircon $\delta^{18}\text{O}$ dataset (Fig. 6) shows an envelope of increasing values from Archean (max = 7.2 ‰) to Paleoproterozoic (max = 11.4 ‰), with average values increasing from 5.8 ‰ to 7.1 ‰. Zircon with high $\delta^{18}\text{O}$ values (> 6.5 ‰) indicate crustal recycling processes (Hawkesworth and Kemp, 2006), having crystallized from a melt with a component of sediments or altered mafic crust. This is consistent with previous trends in zircon $\delta^{18}\text{O}$ interpreted to reflect a secular change in the $\delta^{18}\text{O}$ of subduction-related melts in the aftermath of the Great Oxidation Event (Spencer et al., 2019).

5. Discussion

5.1. Tectonic basin setting

Detrital zircon U–Pb age profiles can unravel the tectonic setting of their depositional basin because the volume of zircon production is a direct reflection of the differences in tectonic processes (e.g., Busby and Ingersoll, 1995; Gehrels, 2014). Magmatism associated with convergent settings will shed zircon grains with ages close to the time of deposition, thus convergent plate margins

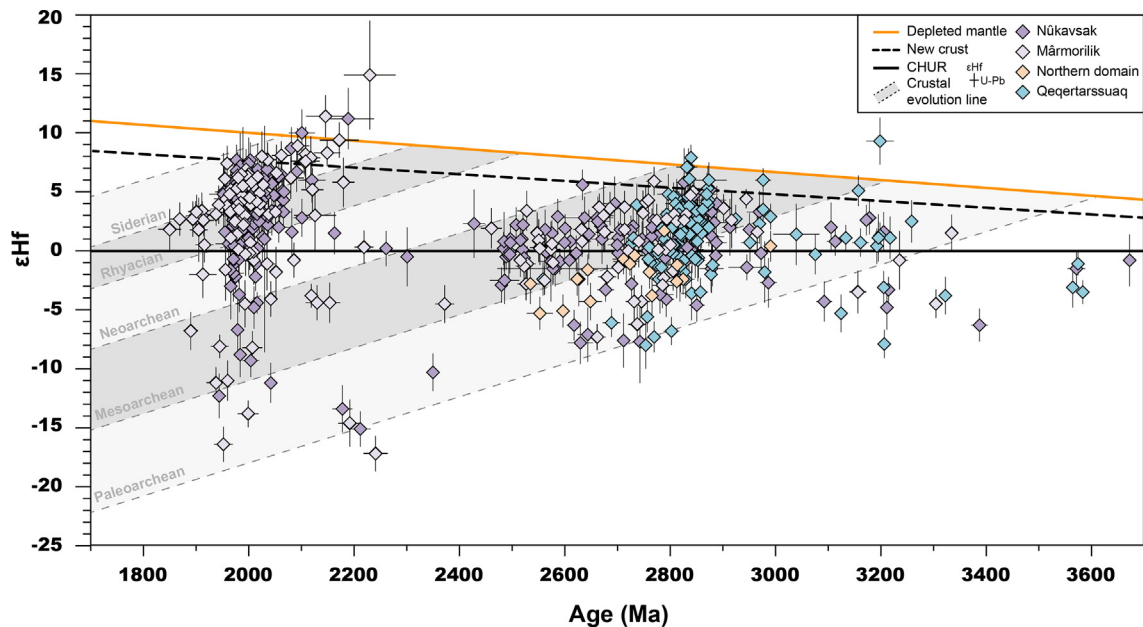


Fig. 5. Detrital zircon U-Pb age vs. ϵ_{Hf} for the Karrat Group (Nûkavsak and Mârmorilik formations), the northern domain metasedimentary rocks (Karrat Group, *sensu lato*), and Qeqertarsuaq complex. Paleoproterozoic zircon in the uppermost Karrat Group (Nûkavsak and Mârmorilik formations) overwhelmingly yield positive ϵ_{Hf} values, suggesting derivation from juvenile ~2150 to 1900 Ma sources. Paleoproterozoic zircon in the northern domain Karrat Group yields exclusively negative ϵ_{Hf} values. The oldest unit, the Qeqertarsuaq complex, contains only Archean grains, with the largest population of positive ϵ_{Hf} values being associated with grain ages between ~2800 and 2870 Ma. Local Archean orthogneisses (~3160 to 2700 Ma) were a source for all four units; however, the Karrat Group shows a transition to a wider Archean provenance in addition to diverse Paleoproterozoic grain ages. Evolution lines are shown for CHUR (chondritic uniform reservoir; [Bouvier et al., 2008](#)), DM (depleted mantle; [Griffin et al., 2004](#)), and NC (new crust; [Dhuime et al., 2011](#)). Crustal evolution lines represent a Lu/Hf ratio of 0.12. Errors for ϵ_{Hf} values and U-Pb ages are ± 2 sigma; average error for the entire dataset shown by symbols in the legend.

show a dominant population of zircon ages close to the depositional age of the sediment, whereas collisional and extensional tectonic settings have a greater proportion of older ages that can reflect the underlying basement ([Cawood et al., 2012](#)). The U-Pb age profiles and estimated depositional ages of sedimentary units in this study, including the Karrat Group (Qaarsukassak, Nûkavsak, Mârmorilik formations), northern domain metasedimentary rocks, and Qeqertarsuaq complex, reveal diverse tectonic settings when plotted in a cumulative probability density diagram that discriminates tectonic setting based on the probability of a certain percentage of zircon grain ages close to its depositional age ([Fig. 7](#)). The Karrat Group units illustrate a progression from an extensional (Qaarsukassak, lower Mârmorilik formations) to a convergent margin basin setting (Nûkavsak, upper Mârmorilik formations). By contrast, the northern domain metasedimentary rocks plot as a collisional basin setting.

Using the < 2660 Ma maximum depositional age, the Qeqertarsuaq complex plotted on such a diagram suggests a collisional basin setting ([Fig. 7](#)). Very little is known about the Archean basement history on the Rae craton of West Greenland. Zircon ϵ_{Hf} values from detrital zircon in this study reveal a dynamic Archean history that significantly expands available data for this region of the Rae craton. The vertical ϵ_{Hf} array in the Qeqertarsuaq data suggests an orogenic event between ca. 2850 and 2750 Ma that has thus far not been documented in the region.

With these broad tectonic settings in mind, as indicated from zircon age population statistics, the provenance of each unit is addressed below. Detrital zircon ages represent an opportunity to track the uplift, erosion, and paleogeography of surrounding mountain systems in collisional settings as well as coeval magmatic activity in convergent settings (e.g., [Cawood et al., 2012](#)), which guides our discussion and contributes to a more accurate reconstruction of surrounding Paleoproterozoic convergent and/or collisional tectonic events proximal to West Greenland.

5.2. Provenance analysis

Potential provenance is identified for the Qeqertarsuaq complex, Karrat Group, and northern domain metasedimentary rocks based on similar U-Pb zircon age peaks and ϵ_{Hf} values on the Rae craton and surrounding terranes/cratons. Paleogeographic maps that reflect the maximum depositional age of the studied units were constructed using GPlates ([Fig. 8](#)).

5.2.1. Provenance for the Qeqertarsuaq complex

The maximum depositional age determined for the Qeqertarsuaq complex in this study is 2658 ± 11 Ma, with a youngest single grain age of 2559 ± 13 Ma out of a total of 394 detrital zircon grains analyzed ([Fig. 4](#), [Supplementary Data Fig. S3](#)). No grain ages younger than ca. 2.6 Ga were found in this study, so we consider the maximum depositional age of the Qeqertarsuaq complex to be ca. 2660 Ma.

Dominant age peaks range from Neoproterozoic to Mesoarchean ca. 2716–2790 Ma, 2740–2855 Ma, and 2800–2865 Ma to 2940–3016 Ma and 2894–3003 Ma, whereas secondary peaks include a range from Mesoarchean to Paleoproterozoic ca. 2960–3260 Ma and 3513–3530 Ma ([Fig. 4](#), [Supplementary Data Fig. S3](#)). Most of these grains can be attributed to ca. 3160–2700 Ma basement ages documented within the immediate area of the Karrat Group ([Thrane, 2021](#)), suggesting an overall local provenance. Although ca. 3.0 Ga and ca. 2.8 Ga basement rocks are known from the Disko Bugt region ([Connelly et al., 2006](#); [Garde and Hollis, 2010](#)) and ca. 2.8 Ga sources from Baffin Island ([Wodicka et al., 2002](#)), as well as the Slave craton, Nova domain, and Caledonides (Isachsen and Bowring, 1997; Mortensen et al., 1988; Northrup et al., 1999; [Thériault and Ross, 1991](#); [Thrane, 2002](#)), it is likely not necessary to invoke those as sources as these peak grain ages can be found in the underlying basement rocks to the Qeqertarsuaq complex listed above.

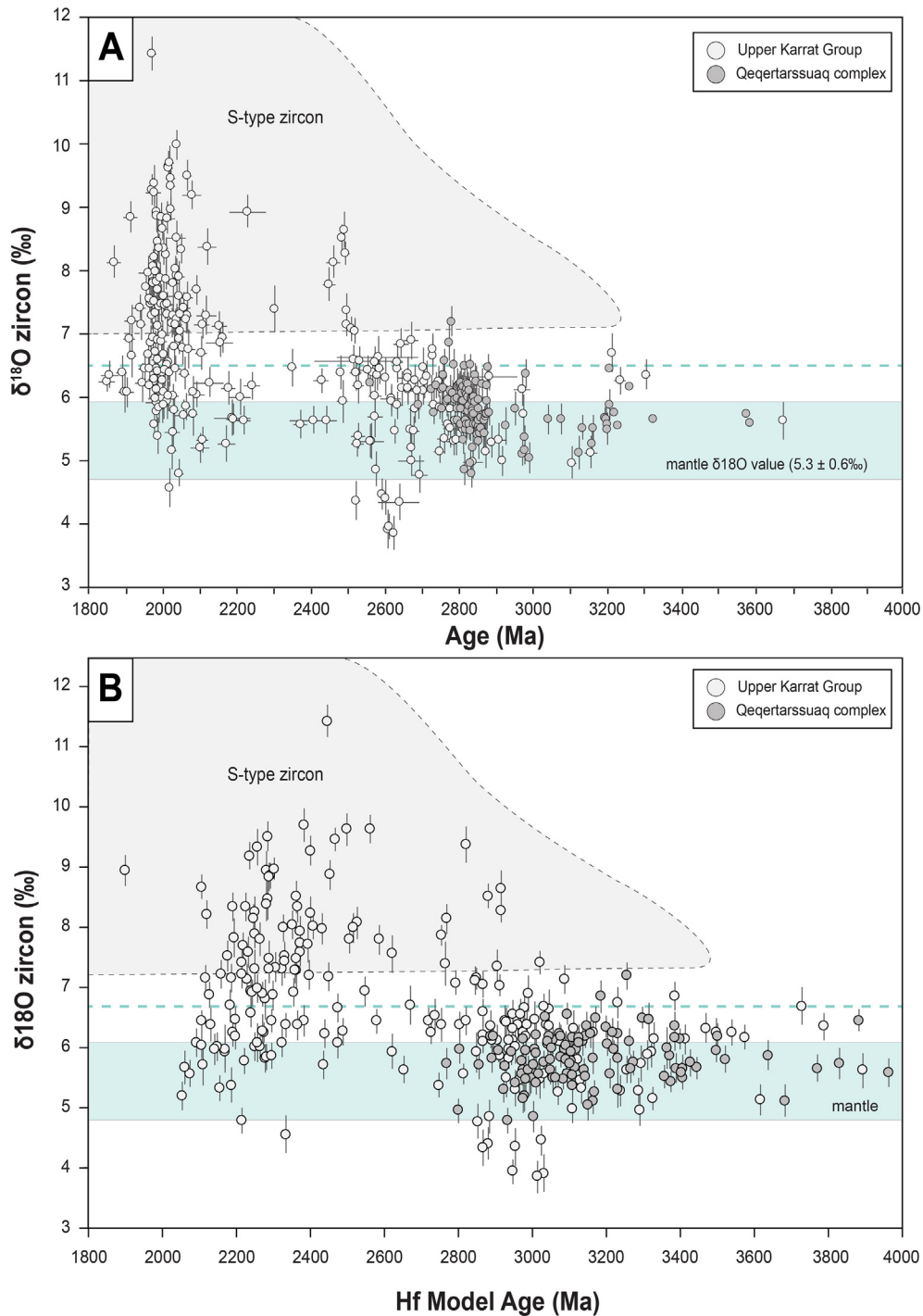


Fig. 6. A. Detrital zircon U-Pb age and $\delta^{18}\text{O}$ value from the upper Karrat Group (Nükavsak and Marmorilik formations, $n = 258$) and the Qeqertarsuaq Formation ($n = 111$). Mantle-equilibrated zircon values (~ 4.7 to 5.9 ‰) from Page et al. (2007). Dashed line ($\delta^{18}\text{O} < 6.5$ ‰) represents magmas crystallized with negligible supracrustal input (e.g., Kemp et al., 2006). Uncertainties for $\delta^{18}\text{O}$ displayed at the 2-sigma level; uncertainties for U-Pb age displayed at the 1-sigma level. Zircon $\delta^{18}\text{O}$ values increase after the Archean-Proterozoic boundary, indicating a supracrustal component to melts with higher $\delta^{18}\text{O}$. B. Depleted mantle Hf model age (T_{DM}) vs. $\delta^{18}\text{O}$ value for detrital zircon from the upper Karrat Group (Nükavsak and Marmorilik formations) and the Qeqertarsuaq Formation. Model ages were calculated using $^{176}\text{Lu}/^{177}\text{Hf} = 0.010$ after Pietranik et al. (2008). Only zircon with concordant U-Pb age data (within ± 10 % discordance) were included for Hf calculations.

Grains as old as ca. 3.6 Ga are documented (e.g., 3584 ± 11 Ma, 3575 ± 12 Ma, 3565 ± 11 Ma from 572830/S4857), however, which have not yet been found locally in the Rae craton of West Greenland. There are few ca. 3.6 Ga provenance locations, which includes the 4.02 – 3.4 Ga Acasta Gneiss complex of the Slave craton (Bauer

et al., 2020). Currently there are insufficient data to confidently identify the 3.6 Ga component identified in the Qeqertarsuaq sediments. Overall, grain ages from the Qeqertarsuaq complex support a dominantly local-derived provenance with some Paleoproterozoic sources not yet identified.

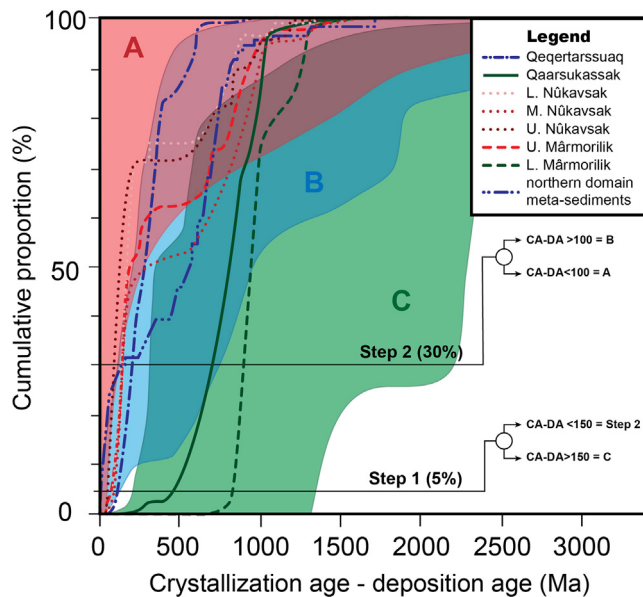


Fig. 7. Tectonic setting inferred from the detrital zircon record of the Karrat Group (Qaarsukassak, Nûkavsak, and Mârmorilik formations), northern domain metasedimentary rocks (Karrat Group, *sensu lato*), and Qeqertarsuaq complex. Extensional basin settings (e.g., rift basin, passive margin, intracratonic basin) are characterized by the youngest 5% of the grain ages with a lag time (crystallization age minus depositional age) of greater than 150 million years of deposition, whereas convergent plate margins (e.g., trench, forearc, backarc basins) the youngest 30% of grain ages with a lag time of less than 100 Myr. Continental collisional settings (e.g., foreland basins) are characterized by the youngest 30% of grain ages with a lag time between 150 and 100 Myr of deposition (Cawood et al., 2012). The Qaarsukassak Formation plots in the extensional basin field, consistent with an intracratonic basin setting/epeiric sea. The Mârmorilik Formation transitions from extensional at the base of the formation to convergent at its stratigraphic top. The Nûkavsak Formation plots in the convergent basin field, regardless of stratigraphic level (MDA: lower Nûkavsak, 1980 Ma; middle Nûkavsak, 1950 Ma, upper Nûkavsak 1900 Ma). The upper Mârmorilik Formation is correlative to the Nûkavsak Formation and also plots in the convergent field. A depositional age ca. 2660 Ma for the Qeqertarsuaq complex results in this unit plotting in the collisional field. At a depositional age of ca. 1920 Ma, the northern domain metasedimentary samples plot in the collisional field.

5.2.2. Provenance for the Qaarsukassak formation

The maximum depositional age determined for the Qaarsukassak Formation is 2006 ± 6.4 Ma, with a single youngest grain age of 1956 ± 18 Ma, out of a total of 797 detrital zircon grains analyzed (Fig. 4, Supplementary Data Fig. S3). Paleoproterozoic grains are relatively minor; however, there are detrital grain ages ranging from ca. 1956 Ma to 2500 Ma ($n = 55$), which differentiates this unit from the older Qeqertarsuaq complex that lacks Paleoproterozoic detritus. The detrital zircon profiles are typically dominated by ca. 2600–2800 Ma or ca. 2900–3000 Ma grains. These ages are consistent with dominantly local provenance: local basement rocks range from ca. 3160 to 2700 Ma (Thrane, 2021; this study). Paleoproterozoic zircon grains mostly comprise grains between ca. 2370 and 2490 Ma; however, there are several ca. 2100, 2160, and 2215–2280 Ma grains, as well as a few around 2000 Ma, which cannot be attributed to known local provenance.

5.2.2.1. Sourcing 2.5–2.3 Ga zircon grains. Plutonic rocks aged <2.5–2.3 Ga are relatively rare on the Rae craton and have not been documented locally on the Rae craton of West Greenland. Rocks of this age were formed during the Arrowsmith orogeny that affected large regions of northern Canada (Berman et al., 2013), with most outcrops being clustered on the western and southwestern Rae craton, including the Taltson basement complex. For the Qaarsukassak Formation, ca. 2370–2490 Ma grains were identified.

The only identified potential provenance sources for these grains is the Taltson basement complex of the Rae craton, which includes ages from ca. 2270 to 2400 Ma (McNicoll et al., 2000; van Breemen et al., 1992).

Notably, the Southern terrane orthogneiss and metaquartzite (Prudhoe Land granulite complex) of the Inglefield mobile belt contain dominant to subdominant ca. 2.4–2.2 Ga zircon populations (Nutman et al., 2008), which differs from the Karrat Group samples documented in this study. This is, however, a common trait shared with Canadian Rae craton supracrustal successions, including the Penrhyn, Piling, and Lake Harbour Groups in addition to many others (see compilation in Partin et al. (2014b)), suggesting that the ca. 2.4–2.2 Ga magmatic and plutonic record was largely recycled into younger Paleoproterozoic metasedimentary successions and is only rarely preserved (Partin et al., 2014b).

5.2.2.2. Sourcing 2.2–2.0 Ga zircon grains. Plutonic rocks aged ca. 2.2–2.0 Ga are relatively rare on the Rae craton and ca. 2.0 Ga ages are generally clustered in the west and south Rae craton. Accordingly, these ages are documented in the Penylan domain (ca. 2050 to 2030 Ma), as well as the Chinchaga-Buffalo Head domain (ca. 2000 Ma, 2017 Ma, 2070 Ma, 2088 Ma, 2160 Ma), Wabamun domain (ca. 2100 Ma), and the Taltson basement complex (ca. 2140 Ma) in the Alberta subsurface (Thériault and Ross, 1991; Villeneuve et al., 1993; Davis et al., 2015). Within the ca. 2070–1960 Ma Thelon tectonic zone, ca. 2030–1960 Ma volcanism and plutonic rocks are interpreted to represent (juvenile) arc magmatism (Davis et al., 2021; Whalen et al., 2018). More proximal on the Melville Peninsula, there are ca. 2150 Ga diorite and 2020 Ma monzogranite intrusions (Wodicka et al., 2011). On the Slave craton, the ca. 2160–2180 Ma Blatchford Lake intrusive suite is another possibility (Mumford, 2013).

All the sources listed above could account for the Paleoproterozoic grains in the Qaarsukassak Formation, with the Chinchaga-Buffalo Head domain capturing potential ca. 2000 Ma, 2090 Ma, and 2160 Ma sources, although ca. 2160 Ma intrusive rocks are documented on the Melville Peninsula and the Slave craton. The Slave craton source is less likely because the timing of its collision with the Rae craton occurred ca. 1.95 Ga (Berman et al., 2023; Cutts and Dyck, 2023). The Ellesmere-Inglefield mobile belt (Laughton et al., 2022; Nutman et al., 2008) was not yet formed, so was not a sediment source for the Qaarsukassak Formation. Similarly, the ca. 2000 Ma granitoids (2007 ± 14 Ma, 2006 ± 21 Ma) on Ellesmere Island (Gilotti et al., 2018) were not likely proximal to the Rae craton of northwest Greenland until ca. 1.93 Ga, well after the maximum depositional age of the Qaarsukassak Formation.

Thus, potential ca. 2370–2490 Ma provenance sources in the Qaarsukassak Formation, as well as ca. 2100, 2160, and 2215–2280 Ma, are most likely derived from the western Rae craton, implying that the Rae craton of Canada was connected to the Rae craton of West Greenland at this time (Fig. 9). This demonstrates that the provenance was not entirely local for the Qaarsukassak Formation and that it received some catchment sourced from topographic highs via river systems across the Rae craton. The Qaarsukassak Formation was deposited in a fluvial to shallow marine environment of an extensional tectonic setting of an epeiric sea, likely an intracratonic or rift basin (Fig. 9).

5.2.3. Provenance for the Nûkavsak and upper Mârmorilik formations

A total of 665 zircon grains with U-Pb data are from the Nûkavsak Formation and a total of 272 are from the upper Mârmorilik Formation in our study (Fig. 4, Supplementary Data Fig. S3). The maximum depositional age determined for the upper Nûkavsak Formation is 1899 ± 10 Ma, which is similar to the maximum depositional age determined for the upper Mârmorilik Formation of 1877 ± 9.5 Ma (Table 1). Detrital zircon spectra are influenced by

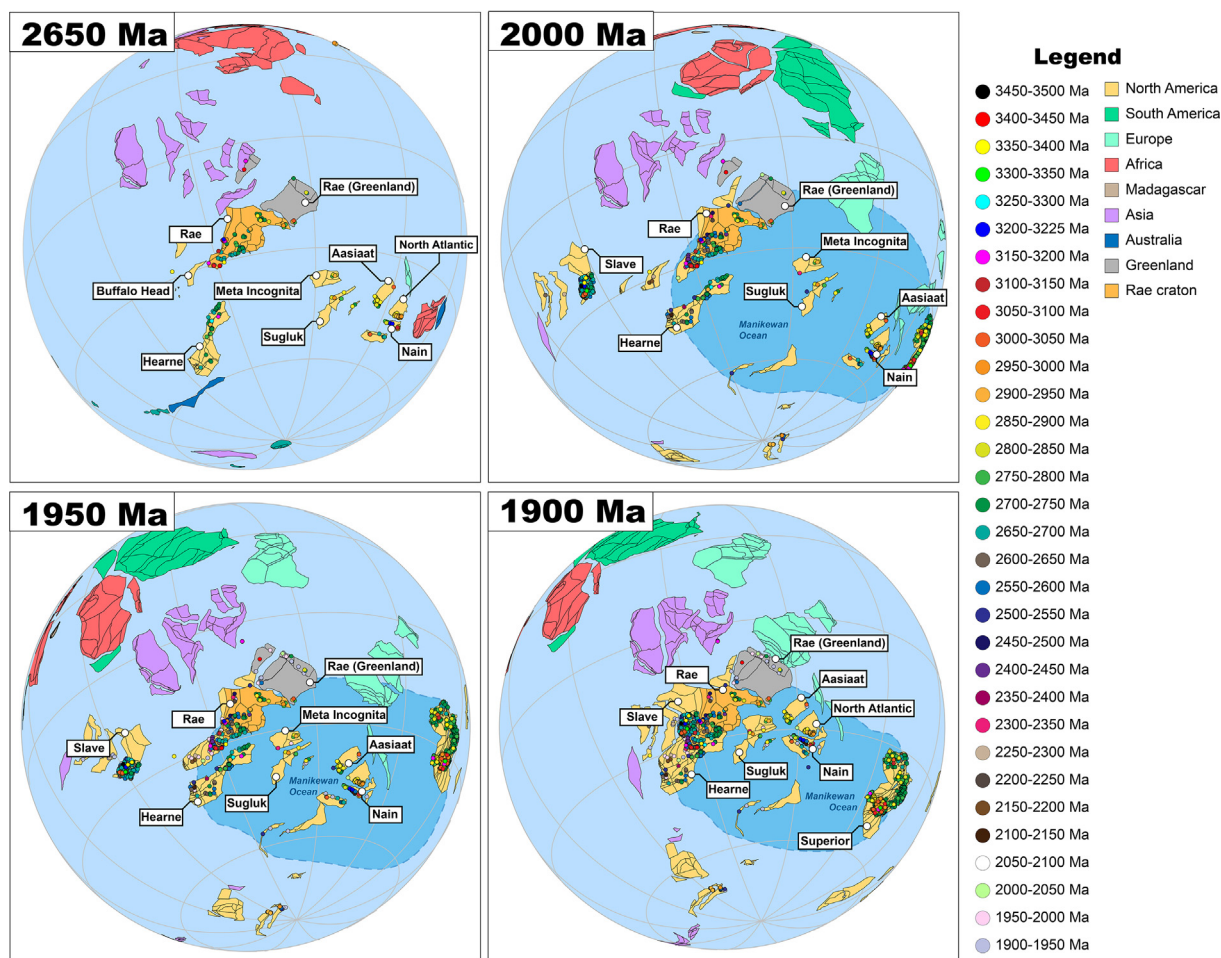


Fig. 8. Plate reconstructions at 2650 Ma, 2000 Ma, 1950 Ma, and 1900 Ma with potential provenance sources (10-million-year bins) as colored circles. Grey polygon is Greenland. Source: GPlates and DateView

many factors that affect their maximum depositional age, from sampling to analysis to variations in catchment (e.g., Fedo et al., 2003), however, we see trends in maximum depositional age based on stratigraphic level (Table 1). Thus, we impose a ca. 1980 Ma maximum depositional age for the lower Nûkavsak Formation, a ca. 1950 Ma maximum depositional age for the middle Nûkavsak Formation, and a ca. 1900 Ma for upper Nûkavsak Formation guided by their stratigraphic position and youngest detrital zircon grains. The progression of tectonic setting from the Qaarsukassak to Nûkavsak/upper Mârmorilik units that allows us to consider that craton-wide tectonic events influenced their detrital zircon profiles. Thus, major tectonic events that occurred after ca. 1.95 Ga, including the Thelon, Taltson, Ellesmere-Inglefield, and Snowbird tectonic events, can be considered as potential sources for the Nûkavsak and upper Mârmorilik formations (Fig. 9). The addition of zircon ϵ_{Hf} data is useful in distinguishing between potential sources of similar age.

The Nûkavsak and upper Mârmorilik formations have overlapping dominant and subdominant U-Pb age peaks, suggesting the two units have similar sources. Though not definitively correlated by Henderson and Pulvertaft (1987), it is interpreted here that these two units are correlative. The detrital zircon profiles of the lower Nûkavsak Formation are typically dominated by ca. 1950–2050 Ma grains with subdominant populations at 2174 Ma, 2560 Ma, 2617–2761 Ma, 2880 Ma, and 3220 Ma (Fig. 4, Supplementary Data Fig. S3). The detrital zircon profiles of the lower-middle Nûkavsak Formation are typically dominated by ca.

1960–2040 Ma grains with subdominant populations at ca. 2085–2114 Ma, 2474–2535 Ma, and 2555–2823 Ma, as well as Mesoarchean grains at 3102 Ma and 3159–3225 Ma. The detrital zircon profiles of the upper Nûkavsak Formation are typically dominated by ca. 1913–2031 Ma grains with subdominant populations at 2542–2613 Ma, 2665–2715, and 2856–2884 Ma. The detrital zircon profiles of the upper Mârmorilik Formation are dominated by ca. 1952–2032 Ma grains with subdominant populations at 1906 Ma, 2658–2747 Ma, 2489–2585 Ma, 2694–2758, and 2784–2855 Ma (Fig. 4, Supplementary Data Fig. S3, Table 1).

The combined primary U-Pb age peak of the Nûkavsak and upper Mârmorilik formations extends between ca. 2.075 and 1.925 Ga, most (81 %) of which show positive ϵ_{Hf} values, with a total range from + 8.7 to –16.4. Some possible source locations on the Rae craton for rocks of these ages include the various subdivisions of the Rae craton, including Taltson, Thelon, Buffalo Head, Ksituan domain, Ellesmere-Inglefield mobile belt, and Caledonides of northeast Greenland. Their provenance is addressed by the dominant grain populations below.

5.2.3.1. Archean provenance. The dominant Archean crustal ages in the Slave craton are ca. 2.7–2.58 Ga, whereas the dominant Archean crustal ages in the Rae craton are ca. 2.50–2.75 with rocks as old as ca. 3.4–3.2 Ga (Fig. 10). There are 3.2–3.3 Ga candidate grains in our dataset with positive ϵ_{Hf} values that match the Perry River terrane of the western Rae craton (Neil et al., 2023). Eoarch-

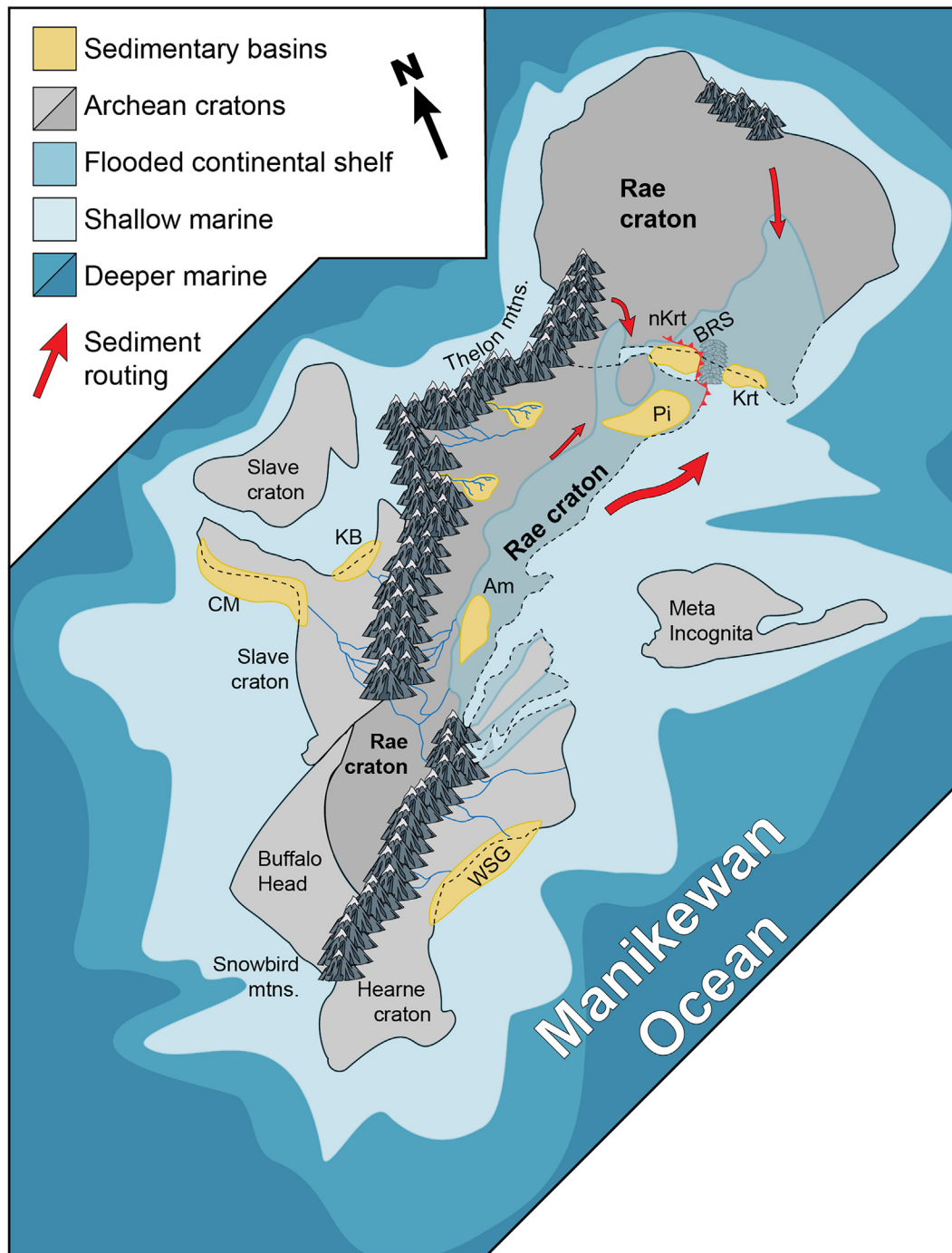


Fig. 9. Envisaged paleotopography of the Rae craton and sediment routing systems for the Karrat basin at ca. 1910 Ma. The erosion of mountains created in various orogenies around its peripheries (including the Thelon, Snowbird, and those in northeast Greenland) would have generated detritus that was routed through fluvial systems into the Karrat basin(s). Abbreviations: Krt, Karrat basin; nKrt, northern Karrat basin; BRS, future Baffin-Rinkian suture; Pi, Piling Group; WSG, Wollaston Supergroup; Am, Amer Group; KB, Kilohigok basin; CM, Coronation margin. Craton configuration from GPlates, which does not yet include the Rinkian-Baffin suture, as its veracity awaits robust paleomagnetic data.

ean U-Pb detrital zircon ages in our dataset (e.g., ca. 3.5 and 3.6 Ga) in the upper Karrat Group could have been sourced from the Slave craton, whereas Mesoarchean and Neoproterozoic zircon ages have sources either locally or from the western Rae craton basement rocks. Neoproterozoic ca. 2.55–2.51 Ga plutons emplaced on Devon Island, as well as metamorphic events at 2.54, 2.47, and 2.30 Ga (Laughton et al., 2022), probably reflect events of the Arrowsmith orogeny. Ca. 2.55–2.51 Ga grains occur in our Nûkavsak and

Mârmorilik datasets, requiring non-local Rae craton sources to explain these ages.

5.2.3.2. Sourcing < 2.2–2.0 Ga zircon grains. The upper Karat Group was deposited after the Thelon (ca. 2.01–1.97 Ga) and Taltson (ca. 1.99–1.96 Ga) tectonic events and the formation of the Ellesmere-Ingfield mobile belt (as old as ca. 2.01–1.99 Ga); thus, these are potential ca. 2.2–2.0 Ga sources in addition to those listed

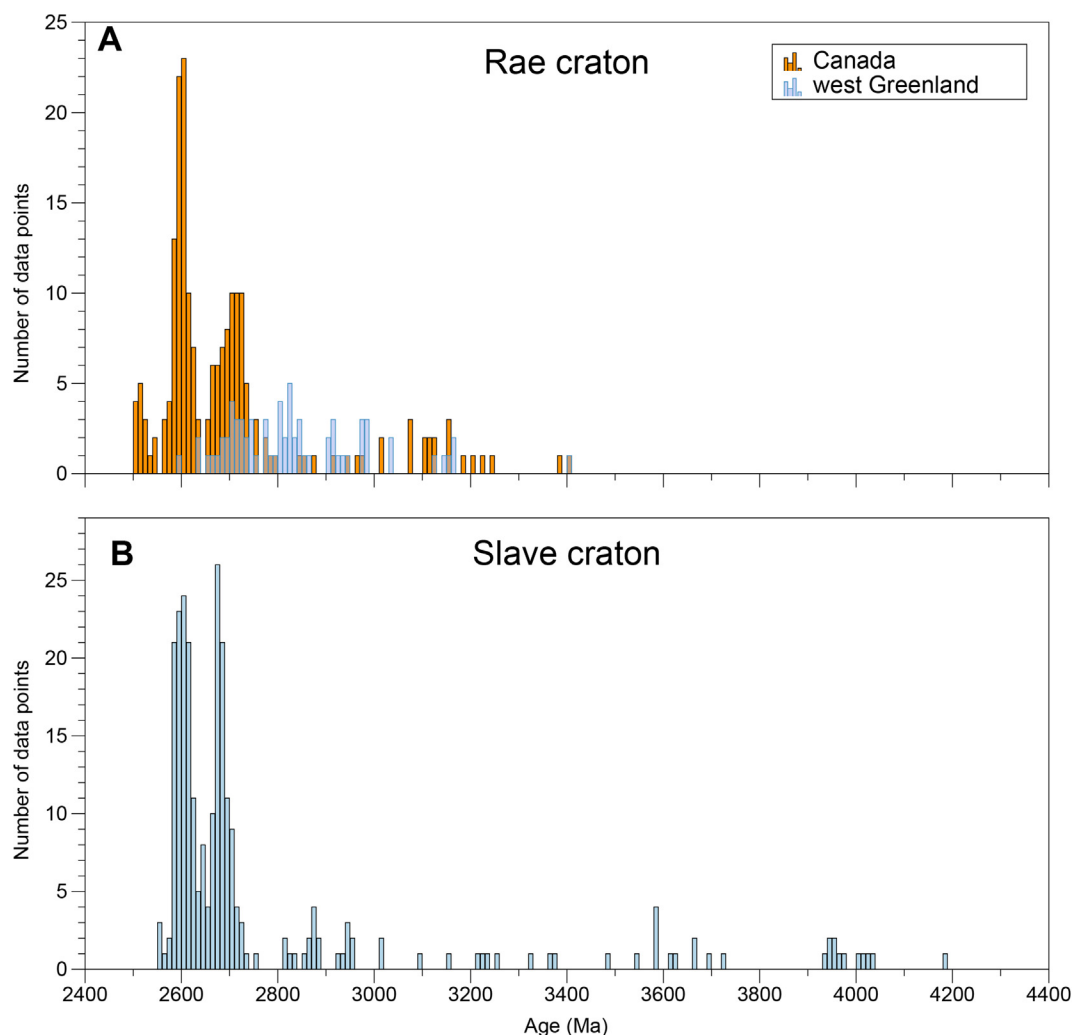


Fig. 10. A. Histogram comparing Archean U-Pb ages of plutonic rocks of the Rae craton from west Greenland (light blue; $n = 71$) and Canada (orange; $n = 199$). B. Histogram comparing Archean U-Pb ages of plutonic rocks of the Slave craton (blue; $n = 264$). Data from Dateview database, Canadian Geochronology Knowledgebase (2013), and Thrane (2021).

above (section 5.2.2). As such, grains aged ca. 2.2–2.0 Ga could be sourced from the western Rae craton, Slave craton, or northern Greenland. Our dataset, however, shows dominantly positive ϵ_{Hf} values (82 %) in ca. 2.2–2.0 Ga zircon, whereas most known rocks of this age from the Rae craton have negative ϵ_{Hf}^* values. The ca. 2160–2180 Ma Blatchford Lake intrusive suite of the Slave craton (Mumford, 2013) with positive ϵ_{Hf}^* values, or possibly the Chinchaga domain of the Rae craton (Thériault and Ross, 1991), are the only known sources to explain juvenile grains of this age in our dataset for the upper Karrat Group. Further addressing the subdominant ca. 2175 Ma zircon population in our samples, these crustal ages are only found in the southwestern Rae and Slave cratons, suggesting that these were important sediment sources for the upper Karrat Group. This sediment routing is more realistic given the new model that the Prøven igneous complex represents a major (later) terrane boundary, and thus it would be difficult to envision how detritus could cross over a magmatic arc.

Zircon populations ca. 2.2–2.15 Ga are typical in several Rae metasedimentary successions, including the upper Penrhyn Group, upper Murmac Bay Group, Rutledge River basin (Taltson magmatic zone), and Montresor Group (Bostock and van Breemen, 1994; Rainbird et al., 2010; Partin et al., 2014a; Shiels et al., 2016). Rocks of this age, however, are a relatively minor component of the currently exposed Rae craton. The ca. 2.2–2.05 Ga zircon ϵ_{Hf} values

from the Penrhyn-Piling groups are dominantly negative, contrasting with ϵ_{Hf} values from the same grain ages from the upper Karrat Group that are dominantly positive (Fig. 11). The source of juvenile ca. 2.15 Ma to 2.0 Ma detritus in the upper Karrat Group remains elusive.

5.2.3.3. Sourcing 2.0–1.90 Ga zircon grains. Rocks aged ca. 2.0–1.90 Ga on the Rae craton occur mostly along its margins, including the ca. 2.01–1.97 Ga Thelon arc and the more evolved ca. 1.99–1.96 Ga intracontinental Taltson plutonism on the western and southern Rae cratons (e.g., Davis et al., 2021), and the ca. 1.98–1.92 Ga Ellesmere-Inglefield mobile belt (e.g., Nutman et al., 2008) and eastern Greenland Caledonidian fold belt. Two “arc-like terranes” were proposed by Nutman et al. (2008)—a poorly-delineated one at ca. 2.0 Ga and another at 1.95–1.92 Ga in the Ellesmere-Inglefield mobile belt. Associated with the younger event is a diorite dated at 1940 ± 13 Ma with a ϵ_{Hf}^* of +4.31 (Nutman et al., 2008). Basement rocks of the northeastern Greenland Caledonides ca. 2020 and 1944 Ma (Kalsbeek et al., 1999; Thrane, 2002) are also potential sources. Although there are no Sm-Nd or Hf isotopic data, ca. 2.0–1.85 Ga calc-alkaline rocks in northeast Greenland are interpreted to represent a magmatic arc terrane that collided with the Rae craton (Kalsbeek et al., 2008).

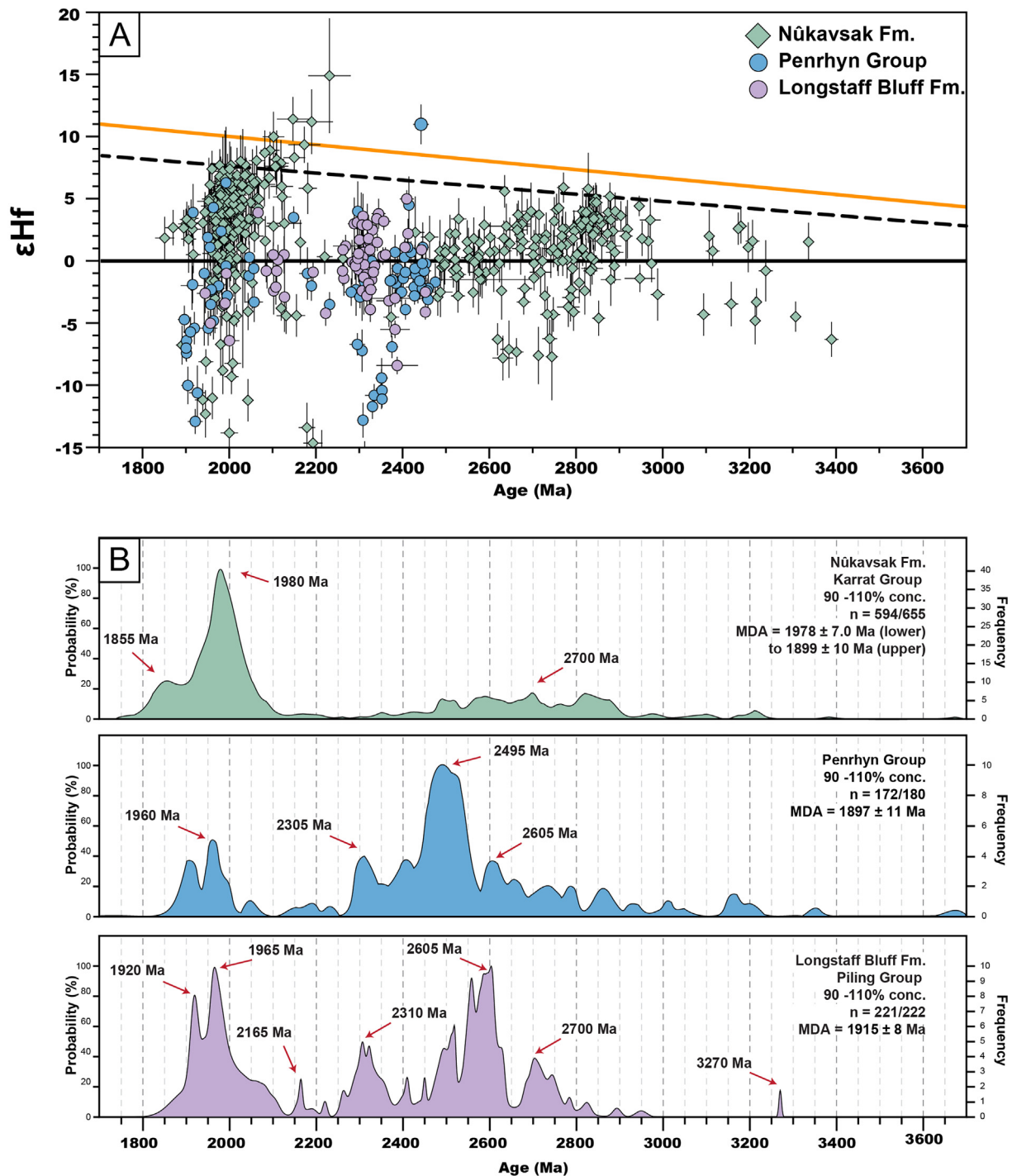


Fig. 11. A. Comparative detrital zircon U-Pb age vs. ϵ_{Hf} for the Nūkavsak Formation (this study), Longstaff Bluff Formation and Penrhyn Group (Partin et al., 2014b; Partin and Sylvester, 2016). B. Comparative combined frequency histogram with normalized probability density curves of detrital zircon U-Pb geochronology from the Nūkavsak Formation (this study), Longstaff Bluff Formation (Partin et al., 2014a; Wodicka et al., 2014), and the Penrhyn Group (Partin et al., 2014a). Maximum depositional ages are: Longstaff Bluff Formation, 1915 ± 8 Ma; Penrhyn Group 1897 ± 11 Ma, Nūkavsak Formation, 1978 ± 7 Ma (lower), 1956 ± 9 Ma (middle), 1899 ± 10 Ma (upper).

The majority (73 %) of ca. 1.95–1.9 Ga zircon grains in our dataset show positive ϵ_{Hf} values, which is in stark contrast with most of the exposed rocks of this age on the Rae craton, which tend to have negative ϵ_{Nd} or ϵ_{Hf} values (e.g., Partin and Sylvester, 2016). There are some negative ϵ_{Hf} values in our dataset (zircon ϵ_{Hf} ranges from +4.8 to –12.3) with which to compare to evolved sources derived from older recycled crust.

Potential sources from the southern and western Rae craton include the Buffalo Head Terrane (ca. 2017–1990 Ma sources with

ϵ_{Hf} values that range from –2.36 to –8.55) and the Ksituan domain (1986 ± 11 Ma and 1987 ± 3 Ma sources with ϵ_{Hf} between –1.58 and –2.04) (Villeneuve et al., 1993). Metamorphic ca. 1.95–1.96 Ga zircon grains can provide another test for the provenance of the Thelon tectonic zone or Taltson magmatic zone. There are no candidate grains with low Th/U ratios identified from the Nūkavsak Formation; however, there are candidate grains in the upper Marmorilik Formation (e.g., 1952 ± 18 Ma; 1955 ± 11 Ma; 1964 ± 12 Ma) that are likely derived from the western Rae craton.

We favor the northeast Greenland Caledonian fold belt as a source for ca. 2000–1940 Ma detritus over the Ellesmere–Inglefield mobile belt to align with the model that accommodates the presence of a subduction zone and magmatic arc (Grocott et al., 2023) that separates the northern and southern Karrat basins. Accordingly, derivation from the western Rae craton sources described above is consistent with this constraint. Thus, zircon ages in our dataset between ca. 2.02 and 1.95 Ga are most reasonably associated with the southern and western Rae craton, and eastern Greenland Caledonian fold belt, considering likely sediment routing systems (Fig. 9).

5.2.3.4. Sourcing ca. 1.9 Ga zircon grains. Grains as young as ca. 1.9 Ga are only captured in the upper Nûkavsak and upper Mårililik formations, signaling a change in source from the deposition of the lower-middle Nûkavsak Formation. Specific sources for this age are somewhat elusive. The Snowbird tectonic zone might provide a potential source for ca. 1900 Ma grains. The Snowbird tectonic zone experienced rapid unroofing starting at ca. 1915 Ma (Cutts et al., 2024). Ca. 1900 Ma magmatic rocks associated with the Snowbird tectonic zone include the 1896 ± 0.3 Ma Chipman mafic dykes (Flowers et al., 2006), a 1900 ± 3.6 Ma syenite in the Snowbird domain (Davis et al., 2015), and the 1902 ± 2 Ma (ϵ_{Hf}^* of 5.5) Kramanitar complex (Sanborn-Barrie et al., 2001). A ca. 1900–1850 Ma volcano-sedimentary trench-arc succession in the Disko Bugt area on the Aasiaat domain (Garde and Hollis, 2010) is a potential source, but was not likely proximal to the Karrat basin during deposition of the Karrat Group.

By ca. 1.92 Ga, juvenile magmatic arcs (e.g., La Ronge, Lynn Lake) were forming in the outboard Manikewan Ocean prior to their accretion onto the southern Rae–Hearne and Superior margins (Ansdell, 2005; Corrigan et al., 2009). Kalsbeek et al. (1998) hypothesized that the youngest grains in the Nûkavsak Formation were sourced from a juvenile magmatic arc that had not yet been documented. We echo this hypothesis, supported by the abundance of positive zircon ϵ_{Hf} in our study, and postulate that an outboard juvenile magmatic arc was the source for the youngest grains in our dataset. Importantly, this is a major difference to be highlighted between the Karrat Group and the Piling and Penrhyn groups of eastern Canada, since ca. 1.95–1.9 Ga zircon ϵ_{Hf} in those metasedimentary rocks are dominated by negative ϵ_{Hf} values (–1 to –12.9, with one value at +3.9) (Partin and Sylvester, 2016). Thus, if upper Karrat Group sediments were sourced, in part, by an outboard juvenile magmatic arc, that arc did not shed into the nearby Piling basin. This is likely a function of the geographical position of the arc. Grocott et al. (2023) postulated erosion of a ca. 2.0–1.95 Ga magmatic arc into both the Piling basin and the Karrat basin(s). Our upper Karrat Group samples do contain abundant juvenile ϵ_{Hf} zircon values, however, they have a wider spread from ca. 2190 to ca. 1950 Ma, requiring an expanded explanation. Additionally, there is no corroborating evidence from detrital zircon ϵ_{Hf} data (Fig. 11) from the Piling Group that arc detritus actually shed into its basin (Partin and Sylvester, 2016)—conflicting with the Grocott et al. model.

Thus, provenance for the upper Karrat Group was dominantly from the west across the Rae craton via continental river systems, which included ca. 1.95 Ga juvenile arc rocks of the Thelon orogen, as well some detritus from the east, sourced from the Caledonian fold belt in northeast Greenland. The sources, however, for the large number of ca. < 1.95–2.15 Ga zircon grains that show positive and depleted-mantle ϵ_{Hf} values in our dataset remain an enigma. Some of these grains (ca. 2.0–1.95 Ga) could be explained by an adjacent magmatic arc, however, another source is required to

explain the ca. 150 Myr of juvenile zircon production from ca. 2.15 to 2.0 Ga.

5.2.4. Provenance for the northern domain metasedimentary rocks (north of Prøven igneous complex)

A total of 411 zircon grains with U–Pb data in our study represents the northern domain Karrat Group (*sensu lato*), which occurs north of the Prøven igneous complex. Both determination of the youngest detrital zircon and provenance analysis for the northern domain metasedimentary rocks are more challenging due to the overall higher metamorphic grade (often granulite facies), as well as small-scale intrusions that were likely analyzed along with detrital zircon (sample 571201). Care was taken to sort out true detrital grains to best assess provenance. For example, the maximum depositional age determined for the northern domain metasedimentary rocks using our initial filtering criteria was at first calculated to be 1914 ± 8.1 Ma (sample 572505). The coupling of Hf isotopes for this sample, however, allowed us to determine that a significant Pb-loss event occurred at ca. 1840 Ma (Supplementary Data Fig. S5). We interpret that the sample originally had only Archean detrital zircon and experienced a Pb-loss event at ca. 1840 Ma such that apparent U–Pb ages cluster from ca. 1920 to 1850 Ma. Although the zircon Hf analyses are robust, the apparent U–Pb ages from Pb-loss for sample 572505 suggests the very low ϵ_{Hf} values (down to –25) are unreliable and thus are not shown on Fig. 5. As such, we assign a ca. 2596 Ma maximum depositional age (Table 1). Using a stricter Th/U ratio cutoff of 0.4, which is more realistic for the higher metamorphic grade of these samples, the maximum depositional age is 1923 ± 10 Ma for sample 571201 and 2438 ± 1.8 Ma for sample 571239. The detrital zircon profiles of the northern domain metasedimentary rocks contain only limited Paleoproterozoic grains ca. 1920–1980 Ma with subdominant populations at ca. 1932 Ma, 2188–2228 Ma, 2490–2666 Ma, and 2720–2820 Ma.

We address the potential sources of the ca. 1920–1980 Ma grains, which could either be from the ca. 2.01 to 1.96 Ga Thelon and Taltson tectonic zones of the western Rae craton, Paleoproterozoic basement rocks of the Caledonides of eastern Greenland (Kalsbeek et al., 1993) for ca. 1945 Ma and 1960 Ma grains, or the ca. 1980–1915 Ma grains could indicate sources from the Ellesmere–Inglefield mobile belt (Fig. 12). The Ellesmere–Inglefield mobile belt would also be a potential source for ca. 1.93–1.92 Ga metamorphic zircon grains that would have been incorporated as detrital zircon into the northern domain sedimentary basin after the collisional events caused the Ellesmere–Inglefield mobile belt to be exhumed. There are a few low Th/U candidate grains in our dataset (1921 ± 27 Ma; 1927 ± 17 Ma; 1935 ± 11 Ma) that meet these criteria; thus, the Ellesmere–Inglefield mobile belt could be a potential sediment source.

A magmatic arc should be the primary source if the northern domain metasedimentary rocks represent a forearc basin, as proposed by Grocott et al. (2023). Uncertainties surrounding the forearc interpretation remain, including that i) this unit does not plot in the convergent margin field on Fig. 7, as would be expected for a forearc basin, ii) its provenance can be explained from sources that do not require arc volcanism (Ellesmere–Inglefield mobile belt and local basement), iii) the scale of the basin is too large for a forearc. Instead, the collisional basin interpretation in Fig. 7, as well as the interpreted provenance here, is consistent with a foreland basin interpretation put forth by Sanborn-Barrie et al. (2017). This, however, hinges on the accuracy of the interpreted maximum depositional age of a single sample (571201) that is otherwise complicated by metamorphism and intrusions. If the true depositional age of the unit is closer to the Proterozoic–Archean boundary



Fig. 12. Histogram comparing U-Pb crystallization ages for plutonic rocks from the Thelon tectonic zone of the western Rae craton (hashed; $n = 34$) and the Ellesmere-Inglefield mobile belt of northwest Greenland (blue; $n = 14$). Data from Canadian Geochronology Knowledgebase (2013), Frisch and Hunt (1993, 1988), Nutman et al. (2008), and Gilotti et al. (2018).

(Table 1), then the basin might be altogether unrelated to the Rinkian orogeny.

5.3. Constraints on orogenic events from zircon Hf, O isotopes

Coupling zircon Hf and O isotopic systems garners an understanding of the magmatic history of the zircon grain; as well, O and Hf isotopic arrays can reveal large scale tectonic events (e.g., Kemp et al., 2006; Collins et al., 2011; Smits et al., 2014). The Lu-Hf composition of zircon is influenced by the potential incorporation of recycled materials (such as metasedimentary rocks, hydrothermally-altered volcanic rocks) or older crustal material into the melt. Zircon O isotopes are useful for distinguishing the influence of recycled crustal materials on the Lu-Hf signal. Mantle-derived magmas have a consistent $\delta^{18}\text{O}$ value ($5.3 \pm 0.6 \text{‰}$) (Valley et al., 1998). This contrasts with magmas that have incorporated sediments (10–40 ‰) or hydrothermally-altered seafloor volcanic rocks (10–20 ‰), which will generally have $\delta^{18}\text{O}$ values $> 6.5 \text{‰}$ (Hawkesworth and Kemp, 2006; Kemp et al., 2006). Granites derived from a metasedimentary component have elevated $\delta^{18}\text{O}$ values $\sim 9\text{--}15 \text{‰}$; although it should be noted that an exception to this has been shown from strongly peraluminous granites (Bucholz and Spencer, 2019). Low $\delta^{18}\text{O}$ magmas reflect remelting, assimilation, or exchange between protoliths or magmas with hydrothermally-altered rocks at high temperatures, including melts generated from hydrothermally-altered gabbros (+2‰ to +5 ‰) from subducted slabs (Valley, 2003; Bindeman et al., 2005; Bindeman, 2008).

Archean zircon grains in our dataset are dominantly associated with mantle-like zircon $\delta^{18}\text{O}$ values (Fig. 6). Rapid crustal growth is thought to have characterized the Meso- and Neoproterozoic eras (e.g., Spencer et al., 2017) and is dominantly represented by granite-greenstone belts that include tonalite-trondhjemite-granodiorite suites. Alternatively, this growth has been progressive (Reimink et al., 2023). Data from zircon Hf arrays have been incorporated into models that distinguish new crustal growth from crustal reworking (e.g., Dhuime et al., 2012). Crustal growth from the Neoproterozoic record in Greenland is not well documented, however. Additionally, the Neoproterozoic sedimentary record is relatively sparse, except for examples like the Slave craton in Canada that contain a high sedimentary to igneous rock ratio (e.g., Henderson,

1981). The provenance of the Qeqertarsuaq complex, as analyzed in this study, is interpreted to be derived from local basement rocks. Therefore, we focus our discussion of the Archean record from the detrital zircon of the Qeqertarsuaq complex as a proxy for local Rae craton basement, whereas Karrat Group units show extrabasinal provenance mixed with local sources. The detrital zircon ϵHf array of the Qeqertarsuaq complex (Fig. 5) shows a characteristic fanning out shape and wide vertical ϵHf array, indicating sampling of a characteristic internal-type (i.e., Alpine–Himalayan–Indonesian type continent–continent collisional) orogen (Collins et al., 2011), which provides insights into the Neoproterozoic history of the Rae craton of west Greenland. The data are mostly concentrated within a ca. 2850 and 2750 vertical ϵHf array, suggesting an orogenic event occurred in the eastern Rae craton at this time. The two orthogneiss samples that represent the Rae craton of West Greenland (Supplementary Data Fig. S4) show dominantly mantle-like $\delta^{18}\text{O}$ values and ϵHf values that range from +6 (depleted mantle-like) to –15 (evolved). Although some grains are likely inherited, the range of zircon ϵHf values in granites can reflect mixed magma sources (e.g., Belousova et al., 2006; Kemp et al., 2007; Sun et al., 2010), as might be expected in either single-source disequilibrium melting, or a collisional orogenic setting (Tang et al., 2014), the latter of which is consistent with the detrital zircon record of the Qeqertarsuaq complex.

Overall, Proterozoic zircon grains in our dataset are associated with both mantle-like zircon $\delta^{18}\text{O}$ values and S-type zircon values (Fig. 6). In general, positive ϵHf values in our dataset are associated with mantle-like zircon $\delta^{18}\text{O}$ values, or those $< 6.5 \text{‰}$ that would indicate supracrustal material was absent from the melt. Shortly after the Archean-Proterozoic boundary, the maximum $\delta^{18}\text{O}$ value in our dataset jumps to 8.65 ‰, representing a step-change in the composition of subduction-related magmatism associated with changes previously identified as being associated with oxygenation of the surface environment (e.g., Spencer et al., 2019). Our Karrat Group dataset lacks abundant ca. 2.4–2.2 Ga detrital zircon grains (unlike the Penrhyn and Piling groups, Fig. 11), so there are not enough data to determine trends in $\delta^{18}\text{O}$ values in this interval; however, the highest $\delta^{18}\text{O}$ value (8.94 ‰) is found in a ca. 2230 Ma grain. The average $\delta^{18}\text{O}$ value for zircon grains older than 2.5 Ga in our dataset is 5.82 ‰, with a maximum value of 7.19 ‰, whereas in grains younger than 2.5 Ga the average $\delta^{18}\text{O}$ is 7.10 ‰,

with a maximum value of 11.43 ‰. This corroborates a step-change in zircon $\delta^{18}\text{O}$ after the Archean-Proterozoic boundary, as first noted by Valley et al. (2005). Conversely, low zircon $\delta^{18}\text{O}$ values are rare in our dataset but are centered around ca. 2638 and 2523 Ma ($n = 7$ grains), ranging from 3.85 to 4.45 ‰. There is a single very low zircon $\delta^{18}\text{O}$ value (1.93 ‰) at ca. 2261 Ma.

Both the Nûkavsak and the upper Mârmorilik formations have dominant detrital zircon age populations between ca. 2190 and 1950 Ma with positive ϵHf values. Zircon with positive ϵHf values clusters mostly between ca. 2080 and 1950 Ma, though there are juvenile zircon grains as old as ca. 2190 Ma. Importantly, the beginning of the cluster of positive ϵHf detrital zircon at ca. 2080 Ma overlaps with the opening of the Manikewan Ocean at ca. 2075 Ma (Ansdell, 2005) and might reflect broader rifting processes across the Rae craton (cf. Rainbird et al., 2010). This is evident in a recent model whereby a Taltson tectonic zone microcontinent rifted off the Rae craton ca. 2.2–2.1 Ga, followed by the development of an accretionary margin along the northern Rae craton ca. 2.01–1.95 Ga (Berman et al., 2023). Our Karrat Group dataset shows more abundant zircon with positive ϵHf values than detrital zircon from the Penrhyn and Piling groups (Fig. 11), which suggests the Karrat basin was a major sink for the ca. 2190–1950 Ma source(s), but the Piling and the younger Penrhyn basins were not.

Thus, a Wilson cycle appears to be recorded in our detrital zircon dataset. Starting around 2190 Ma, the data show highly positive, depleted mantle-like ϵHf values (up to +11.2) that co-occur with highly negative values (down to –14.9). This could be associated with the latest-stage collisional processes of the ca. 2.45–2.26 Ga Arrowsmith orogen, or with rifting associated with the margin of the Rae craton (Berman et al., 2023). The dataset shows another vertical ϵHf array starting ca. 2040 Ma to 1950 Ma with ϵHf values as high as +7.7 at 2036 Ma and as low as –16.4 at 1952 Ma. This is somewhat out-of-step with the timing of the Thelon orogen, which only goes as far back as ca. 2010 Ma in both the western Canada (Davis et al., 2021) and the Inglefield mobile belt (Nutman et al., 2008). Highly positive ϵHf values between 2200 and 2000 Ma currently have no known source.

5.4. Basin analysis and correlation across the Rae craton

The Nûkavsak Formation is interpreted here to represent deposition in a *retro*-arc foreland basin that developed succeeding the back-arc Kangilleq volcanic succession. The extensional tectonics associated with back-arc basin formation can create fault-controlled basins and horsts and grabens, influencing sediment distribution and accumulation patterns, which is seen in some of the lower Nûkavsak Formation and reconciles observations by others (e.g., Grocott and Pulvertaft, 1990) that suggested this unit was deposited in a rift setting. A series of diachronous basins developed whereby sedimentation of Nûkavsak occurred at different times along the foreland system, which explains our geochronology results that trend younger to the south. An analogy can be found in the Appalachian diachronous foreland basin system in the eastern U.S. (e.g., Bradley et al., 2000; Thomas et al., 2017). Diachronous foreland basins exhibit variations in sedimentation patterns along their length due to the sequential uplift and erosion of the mountain belt, but sediment deposition occurs in different parts of the basin at different times. Although sediment in retroarc foreland basins is expected to be primarily derived from the adjacent mountain range or orogenic belt, our provenance analysis shows that sources from a wider geographic area are required to explain our data, which is why we envision this foreland basin in the context of a larger epeiric sea (Fig. 9).

The interpretation of the Foxe fold belt traditionally correlates the Penrhyn-Piling-Karrat groups (Jackson and Taylor, 1972), and

potentially the Anap nunâ Group and the Hoare Bay Group (St-Onge et al., 2009), also on the Rae craton. Testing their correlation requires geochronology to test their timing of deposition and basin closure, as well as documenting their depositional and tectonic settings. If the historical correlation between the Penrhyn, Piling, and Karrat groups is correct, their depositional ages, their basin closure timing, and the provenance of their upper sedimentary units should all be similar. Major differences highlighted below and in Fig. 11 support diachronous opening of the basins in which these sediments were deposited. For example, the Penrhyn Group and the Anap nunâ Group were deposited after ca. 1900 Ma and 1870 Ma, respectively (Connelly et al., 2006; Partin et al., 2014a). By contrast, Piling Group deposition had already ceased by ca. 1897 Ma (Wodicka et al., 2014). It is possible that sub-basins of the Karrat Group closer to the Prøven igneous complex closed by ca. 1900 Ma, with the southern-most sub-basin showing evidence of deposition after 1900 Ma. The relationship between Karrat sub-basins and Maarmorilik sub-basin can be compared to the diachroneity between the Penrhyn and Piling basins. By analogy with diachronous basins developed in the Acadian orogeny (Bradley et al., 2000), the diachroneity of foreland basin initiation and closure along the margin of the Rae craton from Baffin Island to the Melville Peninsula was interpreted to reflect embayments and promontories inherited from the Paleoproterozoic rifting and opening of the Manikewan Ocean (Partin et al., 2014a).

The short-lived < 1.9 Ga Penrhyn Group (Partin et al., 2014a) contrasts with many siliciclastic successions on the Rae craton, which show protracted histories starting at ca. 2.4 or 2.1 Ga and ending with the basin closures associated with ca. 1.92–1.9 Ga orogenic events (Rainbird et al., 2010). The Penrhyn Group contains few ca. 1900 Ma grains and, overall, very few juvenile grains that are younger than 1915 Ma; the majority have very negative ϵHf values in ca. 1980–1900 Ma grains (Partin and Sylvester, 2016). The upper Piling Group (Longstaff Bluff Formation) has no juvenile zircon grains younger than ca. 2075 Ma (Fig. 11). This is in marked contrast to the upper Karrat Group samples (Nûkavsak and Mârmorilik formations) that contain abundant zircon grains with positive ϵHf values from ca. 2150 to 1900 Ma, which represents the dominant age peak in these units. This points to different Paleoproterozoic sources between the Penrhyn, upper Piling, and upper Karrat groups. The upper Piling Group sediments were not sourced from a juvenile arc terrane, whereas the upper Karrat Group undoubtedly had juvenile sources. Within the Karrat Group itself, the Maarmorilik area stratigraphy contains markedly younger grains than any stratigraphy north of it. This leads to a diachronous model of basin opening and closing that demonstrates the migration of the Rinkian orogenic front and foreland basin, in accordance with similarly young ages. The geometry of the Mârmorilik sub-basin is consistent with a broken foreland basin, which form in continental interior regions due to subsidence induced by intra-plate reverse faulting or by mantle flow and interactions with a subducting or underthrusting plate and can be found in both continental collision and subduction-related Andean-type orogens (Horton et al., 2022). The salient feature of a broken foreland basin is a basement-cored block uplift that is either an arch or fault-bounded, which separates the adjacent basins (Horton et al., 2022); this feature is present north of outcrops of the Mârmorilik Formation (Fig. 3).

The stratigraphy and prevailing metamorphic grade of the northern domain Karrat Group (*sensu lato*) contrasts with that of the Karrat Group (*sensu stricto*) south of the Prøven igneous complex (Fig. 2). Their detrital zircon spectra also differ. The northern domain spectra show a ca. 2.4–2.2 Ga mode, whereas the Karrat Group does not (Fig. 4). Although zircon ϵHf data exist for both in our dataset, they cannot be used for comparison due to Pb-loss in the higher metamorphic grade northern domain rocks.

The Karrat Group south of the Prøven igneous complex also contain younger detrital grains overall, which would be expected in the *retro-arc* foreland basin model proposed. These contrasting characteristics suggest it is reasonable to propose that these represent separate sedimentary basins. This can be analogous to the differences between the Penrhyn and Piling groups, for example, that were originally thought to be deposited coevally in the same basin. Notable differences in their stratigraphy (e.g., the Penrhyn Group lacks mafic metavolcanic rocks) as well as their age (Penrhyn Group was deposited after 1897 ± 11 Ma, whereas the Piling basin closed by about the same time, ca. 1897 Ma) refute their correlation and previous assumptions that they were deposited in the same basin (Partin et al., 2014a). The ca. 1.90 Ga continent–continent collision between the Rae craton and the Meta Incognita microcontinent of the Foxe orogeny (Corrigan et al., 2009; St-Onge et al., 2020) did affect both the Penrhyn and Piling basins, but in different ways. While the Piling basin was closed by the creation of the Baffin suture, *syn-orogenic* accommodation was created for the Penrhyn basin.

If the northern domain metasedimentary rocks that occur north of the Prøven igneous complex represent a forearc basin that was deposited adjacent to the Prøven magmatic arc, and the ductile shear zone at Tusssaaq (Escher and Stecher, 1978) represents a terrane boundary, then it need not correlate whatsoever with the Karrat Group (*sensu stricto*) south of the Prøven igneous complex. If the Prøven igneous complex was instead formed via post-collisional delamination, it would be expected to occur much later than the collision itself (typically ca. 40 million years after continent–continent collision, e.g., Harris et al. (1986)), which is inconsistent with geological evidence that points to a later collisional event. In the adjacent ca. 1900 Ma Foxe orogeny, the emplacement of the Cumberland batholith via delamination processes occurred ca. 35–55 million years after continent–continent collision. By contrast, the ca. 1896–1886 Ma Qikiqtarjuaq plutonic suite (St-Onge et al., 2020), which extends across the Baffin suture and is coeval with Rae-Meta Incognita collision in the Foxe orogeny, is arc-derived (Greaney et al., 2018). Thus, the correlation of the Qikiqtarjuaq plutonic suite and the Prøven igneous complex favored by recent geochronology (e.g., Sanborn-Barrie et al., 2017) lends support to an arc-derived origin for the Prøven igneous complex in addition to a revised interpretation of its geochemistry (Grocott et al., 2023).

Arc magmatism proceeded over ca. 200 million years (251–56 Ma) in the Cordilleran arc (e.g., Laskowski et al., 2013), providing an analogue to guide expectations in the Karrat basin detrital zircon age peaks. In fact, the age distribution in our detrital zircon data records phases of arc history whose rock records are not preserved. This includes the interval of juvenile magmatism from ca. 2150 Ma to 1900 Ma recorded in our dataset (Fig. 5), pointing to a Paleoproterozoic arc system adjacent to the Karrat basin.

Using the big-picture tectonic framework and nomenclature of Rainbird et al. (2010) that was applied to Paleoproterozoic sedimentary basins of the Rae craton coupled with the new geochronology in this study, the Karrat Group would represent lithotectonic assemblages 2 (incipient rift) and 3 (epeiric sea) in the Qaarsukassak, lower Marmorilik, and lower Nûkavsak formations and assemblage 4 (foreland basin) in the upper Nûkavsak and upper Marmorilik formations. There are some major differences between Rae craton sedimentary successions in Canada and the Karrat Group in the northeastern Rae craton, including a long-lived unconformity of at least 500 million years between the Qeqertarsuaq complex and the Qaarsukassak Formation, the latter of which infilled paleovalley-type topography (Guarnieri et al., 2016) after ca. 2000 Ma (Fig. 4). Thus, Assemblage 1 is not present in the Rinkian orogen because the Qeqertarsuaq complex represents Archean deposition. The Qaarsukassak Formation is

interpreted here as a marginal marine to marine epicontinental basin, consistent with the epeiric sea of assemblage 3, whereas the lower Marmorilik Formation preserves clear evidence of normal faults developed during rifting. The Nûkavsak Formation and upper Marmorilik Formation were deposited in a shallow to deep marine environment in a retroarc foreland basin setting, consistent with foreland basin development of assemblage 4 during the early stages of the Trans-Hudson orogen. Sedimentation above the basal unconformity of the Karrat Group is characterized by mixed provenance in a foreland basin system, which includes sources that traversed the Rae craton of Canada and Greenland (Fig. 9).

6. Conclusion

We present new zircon U-Pb, Hf, and O isotopes from the ca. 2.0 to 1.87 Ga Paleoproterozoic Karrat Group (*sensu stricto*), northern domain metasedimentary rocks (Karrat Group, *sensu lato*), as well as the ca. 2.6 Ga Qeqertarsuaq complex and basement rocks of the Rae craton of West Greenland. We use these data to show that the provenance of the Karrat Group was a mix of local and extrabasinal, changing from dominantly local provenance in the lower Karrat Group (Qaarsukassak Formation) to more distal provenance in the upper Karrat Group (Nûkavsak and Marmorilik formations). Sources for the Karrat Group (*sensu stricto*) are dominantly from the Rae craton of Canada and Greenland (Figs. 8, 9), including the Thelon-Taltson belt and northeast Greenland. Determining the provenance of the northern domain metasedimentary rocks (Karrat Group, *sensu lato*) is more challenging due to Pb-loss from metamorphism, however, we interpret provenance from the Ellesmere-Inglefield mobile belt and local basement rocks. Accordingly, the tectonic setting of the Karrat Group shows an evolution from an extensional or intracratonic basin setting in an epeiric sea (Qaarsukassak) to a convergent margin setting (lower to upper Nûkavsak and Marmorilik) in the Rinkian orogen. The northern domain metasedimentary rocks could possibly represent a forearc basin, but a foreland basin would be consistent with the collisional basin setting shown in Fig. 7. The high metamorphic grade and poor stratigraphic preservation of the northern domain Karrat Group (*sensu lato*) make the determination of tectonic setting difficult to interpret with stratigraphy alone, making detrital zircon studies valuable. We show that the northern domain metasedimentary rocks were deposited in a separated from the Karrat basin, *sensu stricto*. Thus, because the northern domain metasedimentary rocks and Karrat Group (*sensu stricto*) units are not contiguous and therefore do not follow stratigraphic nomenclature principles (Murphy and Salvador, 1999), we recommend modification to the naming of the northern domain metasedimentary rocks, such as the “Nuussuaq Group”, and renaming the formations within it.

The provenance of the Qeqertarsuaq complex is demonstrably local, derived from surrounding basement rocks, implying that it is autochthonous or parautochthonous. Our U-Pb data show that the Qeqertarsuaq complex represents a collisional-type basin (Fig. 7), which contrasts with previous ideas of a passive margin sequence (e.g., Henderson and Pulvertaft, 1987). Hf isotopes from Archean zircon grains in the Qeqertarsuaq complex reveal a history of juvenile crustal growth in West Greenland that has been previously undocumented. The vertical Hf array is consistent with detritus being derived from an internal type orogen, suggesting that the juvenile magmatism could be derived from a yet undocumented collisional orogenic event. These data should spur future study of Archean rocks of West Greenland.

Zircon Hf isotopes in our Karrat Group dataset identify a Proterozoic Wilson cycle, which includes some previously undocumented juvenile magmatism. Some of this juvenile magmatism (e.g., ca. 2.2–2.0 Ga) has no identified source on the Rae craton,

revealing juvenile magmatism that was eroded and buried into the Karrat sedimentary basin and possibly subducted elsewhere. Younger juvenile magmatism represented in our detrital zircon dataset at ca. 2.00–1.90 Ga is interpreted to represent magmatism associated with juvenile magmatic arcs that developed in the Manikewan Ocean and are otherwise not preserved in the geological record.

The Karrat Group shares some detrital zircon age modes with other sedimentary units of the Rae craton, however one of the major differences is that most of the Karrat Group lacks the prominent ca. 2.4–2.3 Ga detrital zircon mode. This sets it apart from the Penrhyn and Piling groups (Fig. 11). The northern domain Karrat Group (*sensu lato*), however, does contain ca. 2.4–2.3 Ga detritus, which was probably sourced from Arrowsmith-aged rocks along the northern margin of the Rae craton. An additional difference is that while the Penrhyn Group contains few ca. 1900 Ma grains and only a handful of juvenile ca. 2000–1900 Ma grains, and the Piling Group contains neither (Partin and Sylvester, 2016), the upper Karrat Group contains abundant juvenile ca. 2150–1900 Ma grains and is the dominant age peak (Figs. 4, 5), completely unlike the Penrhyn–Piling groups (Fig. 11). These point to key differences in juvenile Paleoproterozoic sources between the Penrhyn, upper Piling, and upper Karrat groups. It should be noted that the Anap nunâ Group also shares a ca. 2.1–1.9 Ga dominant age mode (Connelly et al., 2006), suggesting it could also be sourced from adjacent juvenile arc magmatism, such as the adjacent ca. 1.90–1.85 Ga volcano-sedimentary trench-arc succession near Aasiaat in the Disko Bugt area (Garde and Hollis, 2010).

Karrat basin development differs from that of the Piling, Penrhyn, and Hoare Bay groups in Canada, though they are connected via the Trans-Hudson orogenic system. Accretion of the Meta Incognita microcontinent to the southern margin of the Rae craton ca. 1.9 Ga resulted in syn-orogenic basins along the Rae craton margin, including the Penrhyn basin that received detritus from the Meta Incognita microcontinent (Partin et al., 2014b). The <1.899 Ga Penrhyn Group is younger than both the Piling and Hoare Bay groups, thus records a different syn-orogenic stage than the turbidites of those units. Thus, depositional age differences change the interpretation of their broad correlation—a better analogy is diachronous basins that developed along the Rae continental margin that experienced evolving orogenic fronts, similar to the syn-orogenic basins developed during various stages of the Appalachian orogeny.

CRediT authorship contribution statement

Camille A. Partin: Conceptualization, Formal analysis, Funding acquisition, Investigation, Methodology, Project administration, Resources, Supervision, Validation, Visualization, Writing – original draft, Writing – review & editing. **Brayden S. McDonald:** Formal analysis, Visualization, Writing – review & editing. **Michael McConnell:** Formal analysis, Resources, Validation, Visualization, Writing – original draft. **Kristine Thrane:** Investigation, Methodology, Resources, Validation, Writing – review & editing. **D. Graham Pearson:** Investigation, Validation, Writing – review & editing. **Chiranjeeb Sarkar:** Investigation, Validation. **Yan Luo:** Investigation, Validation. **Richard Stern:** Investigation, Validation, Writing – review & editing.

Declaration of competing interest

The authors declare that they have no known competing financial interests or personal relationships that could have appeared to influence the work reported in this paper.

Acknowledgments

This research was supported by the Geological Survey of Denmark and Greenland and the Ministry of Mineral Resources (Greenland) as part of the Karrat Zinc Project, and the Natural Sciences and Engineering Research Council of Canada (RGPIN-2016-04501 to C.A. Partin) and a Canada Excellence Research Chair award to Pearson. Reviewer Jochen Kolb and one anonymous reviewer are thanked for their contributions in improving the manuscript.

Appendix A. Supplementary material

Supplementary data to this article can be found online at <https://doi.org/10.1016/j.gr.2024.07.011>.

References

- Ansdell, K.M., 2005. Tectonic evolution of the Manitoba-Saskatchewan segment of the Paleoproterozoic Trans-Hudson Orogen. *Canada. Can. J. Earth Sci.* 42, 741–759. <https://doi.org/10.1139/e05-035>.
- Bauer, A.M., Reimink, J.R., Chacko, T., Foley, B.J., Shirey, S.B., Pearson, D.G., 2020. Hafnium isotopes in zircons document the gradual onset of mobile-lid tectonics. *Geochem. Perspect. Lett.* 14, 1–6.
- Belousova, E.A., Griffin, W.L., O'Reilly, S.Y., 2006. Zircon crystal morphology, trace element signatures and Hf isotope composition as a tool for petrogenetic modelling: examples from Eastern Australian Granitoids. *J. Petrol.* 47, 329–353. <https://doi.org/10.1093/ptrology/egi077>.
- Berman, R.G., Pehrsson, S., Davis, W.J., Ryan, J.J., Qui, H., Ashton, K.E., 2013. The Arrowsmith orogeny: geochronological and thermobarometric constraints on its extent and tectonic setting in the Rae craton, with implications for pre-Nuna supercontinent reconstruction. *Precambrian Res.* 232, 44–69. <https://doi.org/10.1016/j.precamres.2012.10.015>.
- Berman, R.G., Cutts, J.A., Davis, W.J., Camacho, A., Sanborn-Barrie, M., Smit, M.A., 2023. The tectonic evolution of Thelon tectonic zone, Canada: a new model based on petrological modeling linked with Lu–Hf garnet and U–Pb accessory mineral geochronology. *Can. J. Earth Sci.* 60, 550–582. <https://doi.org/10.1139/cjes-2022-0147>.
- Bindeman, I., 2008. Oxygen isotopes in mantle and crustal magmas as revealed by single crystal analysis. *Rev. Mineral. Geochem.* 69, 445–478.
- Bindeman, I.N., Eiler, J.M., Yagodinski, G.M., Tatsumi, Y., Stern, C.R., Grove, T.L., Portnyagin, M., Hoernle, K., Danyushevsky, L.V., 2005. Oxygen isotope evidence for slab melting in modern and ancient subduction zones. *Earth Planet. Sci. Lett.* 235, 480–496.
- Bostock, H.H., van Breemen, O., 1994. Ages of detrital and metamorphic zircons and monazites from a pre-Taltson magmatic zone basin at the western margin of Rae Province. *Can. J. Earth Sci.* 31, 1353–1364. <https://doi.org/10.1139/e94-118>.
- Bouvier, A., Vervoort, J.D., Patchett, P.J., 2008. The Lu–Hf and Sm–Nd isotopic composition of CHUR: constraints from unequilibrated chondrites and implications for the bulk composition of terrestrial planets. *Earth Planet. Sci. Lett.* 273, 48–57. <https://doi.org/10.1016/j.epsl.2008.06.010>.
- Bradley, D.C., Tucker, R.D., Lux, D.R., Harris, A.G., McGregor, D.C., 2000. Migration of the Acadian orogen and foreland basin across the northern Appalachians of Maine and adjacent areas (Professional Paper 1624). US Geological Survey.
- Bucholz, C.E., Spencer, C.J., 2019. Strongly peraluminous granites across the Archean-Proterozoic transition. *J. Petrol.* 60, 1299–1348. <https://doi.org/10.1093/ptrology/egz033>.
- Busby, C.J., Ingersoll, R.V. (Eds.), 1995. *Tectonics of Sedimentary Basins*. Blackwell Science.
- Cawood, P.A., Hawkesworth, C.J., Dhuime, B., 2012. Detrital zircon record and tectonic setting. *Geology* 40, 875–878. <https://doi.org/10.1130/G32945.1>.
- Collins, W.J., Belousova, E.A., Kemp, A.I.S., Murphy, J.B., 2011. Two contrasting Phanerozoic orogenic systems revealed by hafnium isotope data. *Nat. Geosci.* 4, 333–337. <https://doi.org/10.1038/ngeo1127>.
- Connelly, J.N., Thrane, K., 2005. Rapid determination of Pb isotopes to define Precambrian allochthonous domains: An example from West Greenland. *Geology* 33, 953–956. <https://doi.org/10.1130/G21720.1>.
- Connelly, J.N., Thrane, K., Krawiec, A.W., Garde, A.A., 2006. Linking the palaeoproterozoic nagssugtoqidian and rinkian orogens through the disko bugt region of West Greenland. *J. Geol.* 163, 319–335.
- Corrigan, D., Scott, D.J., St-Onge, M.R., 2001. Geology of the northern margin of the Trans-Hudson Orogen (Foxe fold belt), central Baffin Island, Nunavut. *Curr. Res.* C23, 1–29.
- Corrigan, D., Pehrsson, S., Wodicka, N., de Kemp, E., 2009. The Palaeoproterozoic Trans-Hudson Orogen: a prototype of modern accretionary processes. *Geol. Soc. Lond. Spec. Publ.* 327, 457–479. <https://doi.org/10.1144/SP327.19>.
- Corrigan, D., van Rooyen, D., Wodicka, N., 2021. Indenter tectonics in the Canadian Shield: a case study for Paleoproterozoic lower crust exhumation, oroclinal development, and lateral extrusion. *Precambrian Res.* 355, 106083. <https://doi.org/10.1016/j.precamres.2020.106083>.

- Cutts, J., Dyck, B., 2023. Incipient collision of the Rae and Slave cratons at ca. 1.95 Ga. *GSA Bull.* 135, 903–914.
- Cutts, J.A., Regis, D., Pehrsson, S.J., Graziani, R., Petts, D.C., Smit, M.A., Knox, B., 2024. Circa 1.9 Ga Rae-Hearne collision from Lu-Hf garnet chronology in eclogites. *Terra Nova*. 10.1111/ter.12709.
- Davis, W.J., Pehrsson, S.J., Percival, J.A., 2015. Results of a U-Pb zircon geochronology transect across the southern Rae craton, Northwest Territories, Canada (Open File No. 7655). Geological Survey of Canada.
- Davis, W.J., Sanborn-Barrie, M., Berman, R.G., Pehrsson, S., 2021. Timing and provenance of Paleoproterozoic supracrustal rocks in the central Thelon tectonic zone, Canada: implications for the tectonic evolution of western Laurentia from ca. 2.1 to 1.9 Ga. *Can. J. Earth Sci.* 58, 378–395. <https://doi.org/10.1139/cjes-2020-0046>.
- Dhuime, B., Hawkesworth, C., Cawood, P., 2011. When continents formed. *Science* 331, 154–155. <https://doi.org/10.1126/science.1201245>.
- Dhuime, B., Hawkesworth, C.J., Cawood, P.A., Storey, C.D., 2012. A change in the geodynamics of continental growth 3 billion years ago. *Science* 335, 1334–1336. <https://doi.org/10.1126/science.1216066>.
- Eglington, B.M., 2004. *DateView: A Windows geochronology database*. *Comput. Geosci.* 30, 847–858.
- Escher, J.C., Stecher, O., 1978. Precambrian geology of the Upernavik-Red Head region (72°15'–75°15' N), northern West Greenland. *Rapp. Grøn. Geol. Unders.* 90, 23–26.
- Escher, A., Watt, W.S., 1976. *Geology of Greenland*. Geological Survey of Greenland Copenhagen.
- Fedo, C.M., Sircombe, K.N., Rainbird, R.H., 2003. Detrital zircon analysis of the sedimentary record. *Rev. Mineral. Geochem.* 53, 277–303. <https://doi.org/10.2113/0530277>.
- Fisher, C.M., Vervoort, J.D., DuFrane, S.A., 2014. Accurate Hf isotope determinations of complex zircons using the “laser ablation split stream” method. *Geochem. Geophys. Geosystems* 15, 121–139.
- Fisher, C.M., Paton, C., Pearson, D.G., Sarkar, C., Luo, Y., Tersmette, D.B., Chacko, T., 2017. Data reduction of laser ablation split-stream (LASS) analyses using newly developed features within ilolite: with applications to Lu-Hf + U-Pb in detrital zircon and Sm-Nd + U-Pb in igneous monazite. *Geochem. Geophys. Geosystems* 18, 4604–4622. <https://doi.org/10.1002/2017GC007187>.
- Flowers, R.M., Bowring, S.A., Williams, M.L., 2006. Timescales and significance of high-pressure, high-temperature metamorphism and mafic dike anatexis, Snowbird tectonic zone, Canada. *Contrib. Mineral. Petrol.* 151, 558–581. <https://doi.org/10.1007/s00410-006-0066-7>.
- Frei, D., Gerdes, A., 2009. Precise and accurate in situ U-Pb dating of zircon with high sample throughput by automated LA-SF-ICP-MS. *Chem. Geol.* 261, 261–270. <https://doi.org/10.1016/j.chemgeo.2008.07.025>.
- Frisch, T., Hunt, P.A., 1993. Reconnaissance U-Pb geochronology of the crystalline core of the Boothia Uplift, District of Franklin, Northwest Territories. *Radiogenic Age Isot. Stud. Rep.*, Geological Survey of Canada Paper 93-2 7, 3–22.
- Frisch, T., Hunt, P.A., 1988. U-Pb zircon and monazite ages from the Precambrian Shield of Ellesmere and Devon Islands, Arctic Archipelago. *Geol. Surv. Can. Pap., Radiogenic Age and Isotopic Studies: Report 2* 88–2, 117–125. <https://doi.org/10.4095/126609>.
- Garde, A.A., 1978. *The Lower Proterozoic Marmorilik Formation, east of Marmorilik, West Greenland*. Nyt Nordisk Forlag.
- Garde, A.A., Hollis, J.A., 2010. A buried Palaeoproterozoic spreading ridge in the northern Nagssugtoqidian orogen, West Greenland. *Geol. Soc. Lond. Spec. Publ.* 338, 213–234. <https://doi.org/10.1144/SP338.11>.
- Gehrels, G., 2014. Detrital Zircon U-Pb Geochronology Applied to Tectonics. *Annu. Rev. Earth Planet. Sci.* 42, 127–149. <https://doi.org/10.1146/annurev-earth-050212-124012>.
- Geological Survey of Canada, 2013. *Canadian Geochronology Knowledgebase*.
- Gilotti, J.A., McClelland, W.C., Piepjohn, K., von Gosen, W., 2018. U-Pb geochronology of Paleoproterozoic gneiss from southeastern Ellesmere Island: implications for displacement estimates on the Wegener fault. *Arktos* 4, 1–18. <https://doi.org/10.1007/s41063-018-0047-x>.
- Greaney, A.T., Rudnick, R.L., Gaschnig, R.M., Whalen, J.B., Luais, B., Clemens, J.D., 2018. Geochemistry of molybdenum in the continental crust. *Geochim. Cosmochim. Acta* 238, 36–54.
- Griffin, W.L., Wang, X., Jackson, S.E., Pearson, N.J., O'Reilly, S.Y., Xu, X., Zhou, X., 2002. Zircon chemistry and magma mixing, SE China: In-situ analysis of Hf isotopes, Tonglu and Pingtan igneous complexes. *Lithos* 61, 237–269. [https://doi.org/10.1016/S0024-4937\(02\)00082-8](https://doi.org/10.1016/S0024-4937(02)00082-8).
- Griffin, W.L., Belousova, E.A., Shee, S.R., Pearson, N.J., O'Reilly, S.Y., 2004. Archean crustal evolution in the northern Yilgarn Craton: U-Pb and Hf-isotope evidence from detrital zircons. *Precambrian Res. Archaean Tecton.* 2 (131), 231–282. <https://doi.org/10.1016/j.precamres.2003.12.011>.
- Grocott, J., Pulvertaft, T.C.R., 1990. The Early Proterozoic Rinkian belt of central West Greenland, in: Lewry, J.F., Stauffer, M.R. (Eds.), *The Early Proterozoic Trans-Hudson Orogen of North America*, *Geol. Assoc. Can., Spec. Pap.* 37, pp. 443–462.
- Grocott, J., Vissers, R., 1984. Field mapping of the early Proterozoic Karrat group on Svartehuk Halvø, central west Greenland.
- Grocott, J., McCaffrey, K.J., 2017. Basin evolution and destruction in an Early Proterozoic continental margin: the Rinkian fold-thrust belt of central West Greenland. *J. Geol. Soc.* 174, 453–467.
- Grocott, J., Thrane, K., McCaffrey, K.J.W., Sleath, P.R., Dziggel, A., 2023. Andean-type, bivergent crustal shortening in the Rinkian orogen: New constraints on the tectonic evolution of Laurentia-West Greenland in the Paleoproterozoic. *Geosphere* 19, 1231–1258. <https://doi.org/10.1130/GES02614.1>.
- Guarnieri, P., Baker, N., 2022. Tectonic inversion of listric normal faults in the foreland of the Rinkian Orogen (Maarmorilik, central West Greenland). *J. Struct. Geol.* 159, 104598. <https://doi.org/10.1016/j.jsg.2022.104598>.
- Guarnieri, P., Baker, N., Rosa, D., Sørensen, E.V., 2022. Geological Map of Greenland 1: 100 000, Maarmorilik 71 V. 2 Syd. Geological Survey of Denmark and Greenland, Copenhagen.
- Guarnieri, P., Partin, C.A., Rosa, D., 2016. Palaeovalleys at the basal unconformity of the Palaeoproterozoic Karrat Group, West Greenland. *Geol. Surv. Den. Greenl. Bull.*, 63–66.
- Guarnieri, P., Rosa, D., Thrane, K., Kokfelt, T.F., Sørensen, E.V., DeWolfe, M.Y., Baker, N., 2023. Tectonics of the Paleoproterozoic Rinkian orogen, central West Greenland. *GSA Bull.* <https://doi.org/10.1130/B36930.1>.
- Harris, N.B.W., Pearce, J.A., Tindle, A.G., 1986. Geochemical characteristics of collision-zone magmatism. *Geol. Soc. Lond. Spec. Publ.* 19, 67–81. <https://doi.org/10.1144/GSL.SP.1986.019.01.04>.
- Hawkesworth, C.J., Kemp, A.I.S., 2006. Using hafnium and oxygen isotopes in zircons to unravel the record of crustal evolution. *Chem. Geol.* 226, 144–162. <https://doi.org/10.1016/j.chemgeo.2005.09.018>.
- Henderson, G., Pulvertaft, T.C.R., 1987. The lithostratigraphy and structure of a Lower Proterozoic dome and nappe complex, descriptive text to 1: 100,000 sheets, Marmorilik 71 V. 2 Syd, Nūgūtsiaq 71 V. 2 Nord and Pangnertōq 72 V. 2 Syd. Geological Survey of Greenland, Copenhagen.
- Henderson, G., Pulvertaft, T.C.R., 1967. The stratigraphy and structure of the Precambrian rocks of the Umanak area, West Greenland. *Meddelelser Fra Dan. Geol. Foren.* 17, 1–20.
- Horton, B.K., Capaldi, T.N., Mackaman-Lofland, C., Perez, N.D., Bush, M.A., Fuentes, F., Constenius, K.N., 2022. Broken foreland basins and the influence of subduction dynamics, tectonic inheritance, and mechanical triggers. *Earth-Sci. Rev.* 234, 104193. <https://doi.org/10.1016/j.earscirev.2022.104193>.
- Hoskin, P.W.O., Schaltegger, U., 2003. The composition of zircon and igneous and metamorphic petrogenesis. *Rev. Mineral. Geochem.* 53, 27–62. <https://doi.org/10.2113/0530027>.
- Jackson, G.D., Taylor, F.C., 1972. Correlation of major orophic rock units in the Northeastern Canadian Shield. *Can. J. Earth Sci.* 9, 1650–1669. <https://doi.org/10.1139/e72-146>.
- Kalsbeek, F., Nutman, A.P., Taylor, P.N., 1993. Palaeoproterozoic basement province in the Caledonian fold belt of North-East Greenland. *Precambrian Res.* 63, 163–178.
- Kalsbeek, F., Pulvertaft, T.C.R., Nutman, A.P., 1998. Geochemistry, age and origin of metagreywackes from the Palaeoproterozoic Karrat Group, Rinkian Belt, West Greenland. *Precambrian Res.* 91, 383–399. [https://doi.org/10.1016/S0301-9268\(98\)00059-X](https://doi.org/10.1016/S0301-9268(98)00059-X).
- Kalsbeek, F., Nutman, A.P., Escher, J.C., Friderichsen, J.D., Hull, J.M., Jones, K.A., Pedersen, S.A.S., 1999. Geochronology of granitic and supracrustal rocks from the northern part of the East Greenland Caledonides: ion microprobe U-Pb zircon ages. *Geol. Greenl. Surv. Bull.* 184, 31–48.
- Kalsbeek, F., Thrane, K., Higgins, A.K., Jepsen, H.F., Leslie, A.G., Nutman, A.P., Frei, R., 2008. Polyorogenic history of the East Greenland Caledonides. *Greenl. Caledonides Evol. Northeast Margin Laurentia Geol. Soc. Am. Mem.* 202, 55–72.
- Kemp, A.I.S., Hawkesworth, C.J., Paterson, B.A., Kinny, P.D., 2006. Episodic growth of the Gondwana supercontinent from hafnium and oxygen isotopes in zircon. *Nature* 439, 580–583. <https://doi.org/10.1038/nature04505>.
- Kemp, A.I.S., Hawkesworth, C.J., Foster, G.L., Paterson, B.A., Woodhead, J.D., Hergt, J.M., Gray, C.M., Whitehouse, M.J., 2007. Magmatic and crustal differentiation history of granitic rocks from Hf-O isotopes in zircon. *Science* 315, 980–983. <https://doi.org/10.1126/science.1136154>.
- Kirkland, C.L., Hollis, J., Danišik, M., Petersen, J., Evans, N.J., McDonald, B.J., 2017. Apatite and titanite from the Karrat Group, Greenland; implications for charting the thermal evolution of crust from the U-Pb geochronology of common Pb bearing phases. *Precambrian Res.* 300, 107–120.
- Kolb, J., 2014. Structure of the palaeoproterozoic nagssugtoqidian orogen, South-East Greenland: Model for the tectonic evolution. *Adv. Underst. Early Precambrian Gneiss Complexes* 255, 809–822. <https://doi.org/10.1016/j.precamres.2013.12.015>.
- Kolb, J., Keiding, J.K., Steenfelt, A., Secher, K., Keulen, N., Rosa, D., Stensgaard, B.M., 2016. Metallogeny of Greenland. *Ore Geol. Rev.* 78, 493–555. <https://doi.org/10.1016/j.oregeorev.2016.03.006>.
- Laskowski, A.K., DeCelles, P.G., Gehrels, G.E., 2013. Detrital zircon geochronology of Cordilleran retroarc foreland basin strata, western North America. *Tectonics* 32, 1027–1048.
- Laughton, J., Osinski, G.R., Yakymchuk, C., 2022. Late Neoproterozoic terrane and Paleoproterozoic HT-UHT metamorphism on southern Devon Island. *Canadian Arctic. Precambrian Res.* 377, 106718. <https://doi.org/10.1016/j.precamres.2022.106718>.
- McNicol, V.J., Thériault, R.J., McDonough, M.R., 2000. Taltson basement gneissic rocks: U-Pb and Nd isotopic constraints on the basement to the Paleoproterozoic Taltson magmatic zone, northeastern Alberta. *Can. J. Earth Sci.* 37, 1575–1596. <https://doi.org/10.1139/e00-034>.
- Mumford, T.R., 2013. *Petrology of the Blatchford Lake Intrusive Suite, Northwest Territories, Canada* (Ph.D. dissertation). Carleton University, Ottawa.
- Murphy, M.A., Salvador, A., 1999. *International stratigraphic guide—an abridged version*. *Episodes J. Int. Geosci.* 22, 255–271.
- Neil, B.J.C., Tersmette, D.B., Chacko, T., Heaman, L.M., Kjarsgaard, B.A., Martel, E., Creaser, R.A., Pearson, D.G., Stern, R.A., Dufrane, S.A., Luo, Y., 2023. Discovery of a giant 3.3–3.1 Ga terrane in the Rae craton, Canada: Implications for the timing

- and extent of ancient continental growth. *Geology* 51, 597–601. <https://doi.org/10.1130/G51110.1>.
- Nutman, A.P., Dawes, P.R., Kalsbeek, F., Hamilton, M.A., 2008. Palaeoproterozoic and Archaean gneiss complexes in northern Greenland: Palaeoproterozoic terrane assembly in the High Arctic. *Precambrian Res.* 161, 419–451. <https://doi.org/10.1016/j.precamres.2007.09.006>.
- Page, F.Z., Fu, B., Kita, N.T., Fournelle, J., Spicuzza, M.J., Schulze, D.J., Viljoen, F., Basei, M.A.S., Valley, J.W., 2007. Zircons from kimberlite: New insights from oxygen isotopes, trace elements, and Ti in zircon thermometry. *Geochim. Cosmochim. Acta* 71, 3887–3903. <https://doi.org/10.1016/j.gca.2007.04.031>.
- Partin, C.A., Bekker, A., Corrigan, D., Modeland, S., Francis, D., Davis, D.W., 2014a. Sedimentological and geochemical basin analysis of the Paleoproterozoic Penrhyn and Piling groups of Arctic Canada. *Precambrian Res.* 251, 80–101. <https://doi.org/10.1016/j.precamres.2014.06.010>.
- Partin, C.A., Bekker, A., Sylvester, P.J., Wodicka, N., Stern, R.A., Chacko, T., Heaman, L.M., 2014b. Filling in the juvenile magmatic gap: Evidence for uninterrupted Paleoproterozoic plate tectonics. *Earth Planet. Sci. Lett.* 388, 123–133. <https://doi.org/10.1016/j.epsl.2013.11.041>.
- Partin, C.A., Sylvester, P.J., 2016. Variations in zircon Hf isotopes support earliest Proterozoic Wilson cycle tectonics on the Canadian Shield. *Precambrian Res.* 280, 279–289. <https://doi.org/10.1016/j.precamres.2016.05.008>.
- Partin, C.A., 2018. Stratigraphy and depositional environment of the Paleoproterozoic Karrat Group, West Greenland. Presented at the Resources for Future Generations, Vancouver, British Columbia.
- Pedersen, F.D., 1980. Remobilization of the massive sulfide ore of the Black Angel Mine, central West Greenland. *Econ. Geol.* 75, 1022–1041.
- Pietranik, A.B., Hawkesworth, C.J., Storey, C.D., Kemp, A.I.S., Sircombe, K.N., Whitehouse, M.J., Bleeker, W., 2008. Episodic, mafic crust formation from 4.5 to 2.8 Ga: New evidence from detrital zircons, Slave craton, Canada. *Geology* 36, 875–878. <https://doi.org/10.1130/G24861A.1>.
- Pulvertaft, T.C.R., 1973. Recumbent folding and flat-lying structure in the Precambrian of northern West Greenland. *Philos. Trans. r. Soc. Lond. Ser. Math. Phys. Sci.*, 535–545.
- Rainbird, R.H., Davis, W.J., Pehrsson, S.J., Wodicka, N., Rayner, N., Skulski, T., 2010. Early Paleoproterozoic supracrustal assemblages of the Rae domain, Nunavut, Canada: Intracratonic basin development during supercontinent break-up and assembly. *Precambrian Res.* 181, 167–186. <https://doi.org/10.1016/j.precamres.2010.06.005>.
- Rayner, N.M., 2017. U-Pb zircon geochronology constraints on timing of plutonism and sedimentary provenance from the Clearwater Fiord-Sylvia Grinnell Lake area. Geological Survey of Canada. southern Baffin Island, Nunavut (Open File Report No. Open File 8204).
- Rayner, N., Sanborn-Barrie, M., Young, M., Whalen, J.B., 2012. U-Pb ages of Archean basement and Paleoproterozoic plutonic rocks, southern Cumberland Peninsula, eastern Baffin Island. *Curr. Res.* 8, 1–28.
- Reimink, J.R., Davies, J., Moyer, J.F., Pearson, D.G., 2023. A whole-lithosphere view of continental growth. *Geochem. Perspect. Lett.* 26, 45–49.
- Rosa, D., Schneider, J., Chiaradia, M., 2016. Timing and metal sources for carbonate-hosted Zn-Pb mineralization in the Franklinian Basin (North Greenland): Constraints from Rb-Sr and Pb isotopes. *Ore Geol. Rev.* 79, 392–407. <https://doi.org/10.1016/j.oregeorev.2016.05.020>.
- Rosa, D., DeWolfe, Y.M., Guarnieri, P., Kolb, J., Laflamme, C., Partin, C.A., Salehi, S., Sørensen, E., Thaarup, S., Thrane, K., Zimmermann, R., 2017. Architecture and mineral potential of the Paleoproterozoic Karrat Group, West Greenland - Results of the 2016 season. *Dan. Og Grøn. Geol. Unders. Rapp.* 5, 112.
- Rosa, D., Bernstein, S., DeWolfe, Y.M., Dziggel, A., Grocott, J., Guarnieri, P., Kolb, J., Partin, C.A., Sørensen, E., Zimmermann, R., 2018. Architecture and mineral potential of the Paleoproterozoic Karrat Group, West Greenland - Results of the 2017 season. *Dan. Og Grøn. Geol. Unders. Rapp.* 23, 102.
- Sanborn-Barrie, M., Thrane, K., Wodicka, N., Rayner, N., 2017. The Laurentia-West Greenland connection at 1.9 Ga: new insights from the Rinkian fold belt. *Gondwana Res.* 51, 289–309.
- Shiels, C., Partin, C.A., Eglinton, B.M., 2016. Provenance approaches in polydeformed metasedimentary successions: Determining nearest neighboring cratons during the deposition of the Paleoproterozoic Murmac Bay Group. *Lithosphere* 8, 519. <https://doi.org/10.1130/L537.1>.
- Sidgren, A.-S., Page, L., Garde, A.A., 2006. New hornblende and muscovite $^{40}\text{Ar}/^{39}\text{Ar}$ cooling ages in the central Rinkian fold belt, West Greenland. *Geol. Surv. Den. Greenl. GEUS Bull.* 11, 115–124.
- Smits, R.G., Collins, W.J., Hand, M., Dutch, R., Payne, J., 2014. A Proterozoic Wilson cycle identified by Hf isotopes in central Australia: Implications for the assembly of Proterozoic Australia and Rodinia. *Geology* 42, 231–234. <https://doi.org/10.1130/G35112.1>.
- Söderlund, U., Patchett, P.J., Vervoort, J.D., Isachsen, C.E., 2004. The ^{176}Lu decay constant determined by Lu-Hf and U-Pb isotope systematics of Precambrian mafic intrusions. *Earth Planet. Sci. Lett.* 219, 311–324. [https://doi.org/10.1016/S0012-821X\(04\)00012-3](https://doi.org/10.1016/S0012-821X(04)00012-3).
- Spencer, C.J., Roberts, N.M.W., Santosh, M., 2017. Growth, destruction, and preservation of Earth's continental crust. *Earth-Sci. Rev.* 172, 87–106. <https://doi.org/10.1016/j.earscirev.2017.07.013>.
- Spencer, C.J., Partin, C.A., Kirkland, C.L., Raub, T.D., Liebmann, J., Stern, R.A., 2019. Paleoproterozoic increase in zircon $\delta^{18}\text{O}$ driven by rapid emergence of continental crust. *Geochim. Cosmochim. Acta* 257, 16–25. <https://doi.org/10.1016/j.gca.2019.04.016>.
- St-Onge, M.R., Scott, D.J., Rayner, N., Sanborn-Barrie, M., Skipton, D.R., Saumur, B.M., Wodicka, N., Weller, O.M., 2020. Archean and Paleoproterozoic cratonic rocks of Baffin Island, in: Geological Synthesis of Baffin Island (Nunavut) and the Labrador-Baffin Seaway, Geological Survey of Canada Bulletin. Geological Survey of Canada, pp. 1–29.
- St-Onge, M.R., Van Gool, J.A.M., Garde, A.A., Scott, D.J., 2009. Correlation of Archean and Paleoproterozoic units between northeastern Canada and western Greenland: constraining the pre-collisional upper plate accretionary history of the Trans-Hudson orogen. *Geol. Soc. Lond. Spec. Publ.* 318, 193–235. <https://doi.org/10.1144/SP318.7>.
- Sun, J.-F., Yang, J.-H., Wu, F.-Y., Li, X.-H., Yang, Y.-H., Xie, L.-W., Wilde, S.A., 2010. Magma mixing controlling the origin of the Early Cretaceous Fangshan granitic pluton, North China Craton: In situ U-Pb age and Sr-, Nd-, Hf- and O-isotope evidence. *Lithos* 120, 421–438. <https://doi.org/10.1016/j.lithos.2010.09.002>.
- Tang, M., Wang, X.-L., Shu, X.-J., Wang, D., Yang, T., Gopon, P., 2014. Hafnium isotopic heterogeneity in zircons from granitic rocks: Geochemical evaluation and modeling of “zircon effect” in crustal anatexis. *Earth Planet. Sci. Lett.* 389, 188–199.
- Thériault, R.J., Ross, G.M., 1991. Nd isotopic evidence for crustal recycling in the ca. 2.0 Ga subsurface of western Canada. *Can. J. Earth Sci.* 28, 1140–1147. <https://doi.org/10.1139/e91-104>.
- Thomas, W.A., Gehrels, G.E., Greb, S.F., Nadon, G.C., Satkoski, A.M., Romero, M.C., 2017. Detrital zircons and sediment dispersal in the Appalachian foreland. *Geosphere* 13, 2206–2230.
- Thrane, K., 2002. Relationships between Archean and Paleoproterozoic crystalline basement complexes in the southern part of the East Greenland Caledonides: an ion microprobe study. *Precambrian Res.* 113, 19–42. [https://doi.org/10.1016/S0301-9268\(01\)00198-X](https://doi.org/10.1016/S0301-9268(01)00198-X).
- Thrane, K., 2021. The oldest part of the Rae craton identified in western Greenland. *Precambrian Res.* 357, 106139. <https://doi.org/10.1016/j.precamres.2021.106139>.
- Thrane, K., Baker, J., Connelly, J., Nutman, A., 2005. Age, petrogenesis and metamorphism of the syn-collisional Proven Igneous Complex, West Greenland. *Contrib. Mineral. Petrol.* 149, 541–555. <https://doi.org/10.1007/s00410-005-0660-0>.
- Valley, J.W., 2003. Oxygen Isotopes in Zircon. *Rev. Mineral. Geochem.* 53, 343–385. <https://doi.org/10.2113/0530343>.
- Valley, J.W., Kinny, P.D., Schulze, D.J., Spicuzza, M.J., 1998. Zircon megacrysts from kimberlite: oxygen isotope variability among mantle melts. *Contrib. Mineral. Petrol.* 133, 1–11. <https://doi.org/10.1007/s004100050432>.
- Valley, J., Lackey, J., Cavosie, A., Clechenko, C., Spicuzza, M., Basei, M., Bindeman, I., Ferreira, V., Sial, A., King, E., Peck, W., Sinha, A., Wei, C., 2005. 4.4 billion years of crustal maturation: oxygen isotope ratios of magmatic zircon. *Contrib. Mineral. Petrol.* 150, 561–580. <https://doi.org/10.1007/s00410-005-0025-8>.
- van Breemen, O., Bostock, H.H., Loveridge, W.D., 1992. Geochronology of granites along the margin of the northern Taltson magmatic zone and western Rae Province, Northwest Territories. *Geol. Surv. Can. Pap.*, 91–92.
- van Gool, J.A., Connelly, J.N., Marker, M., Mengel, F.C., 2002. The Nagssugtoqidian Orogen of West Greenland: tectonic evolution and regional correlations from a West Greenland perspective. *Can. J. Earth Sci.* 39, 665–686.
- Vervoort, J.D., Plank, T., Prytulak, J., 2011. The Hf-Nd isotopic composition of marine sediments. *Geochim. Cosmochim. Acta* 75, 5903–5926. <https://doi.org/10.1016/j.gca.2011.07.046>.
- Villeneuve, M., Ross, G.M., Thériault, R.J., Miles, M., Parrish, R.R., Broome, J., 1993. Tectonic subdivision and U-Pb geochronology of the crystalline basement of the Alberta basin, Western Canada. *Geol. Surv. Can. Bull.* 447, 93.
- Whalen, J.B., Berman, R.G., Davis, W.J., Sanborn-Barrie, M., Nadeau, L., 2018. Bedrock geochemistry of the central Thelon tectonic zone, Nunavut. Geological Survey of Canada.
- Wodicka, N., Corrigan, D., Nadeau, L., Erdmann, S., 2011. New U-Pb geochronological results from Melville Peninsula: Unravelling the Archean and Early Paleoproterozoic magmatic history of the north-central Rae Craton. *Geol. Assoc. Can. Annu. Meet. (abstract)* 34, 59.
- Wodicka, N., St-Onge, M.R., Scott, D.J., Corrigan, D., 2002. Preliminary report on the U-Pb geochronology of the northern margin of the Trans-Hudson Orogen, central Baffin Island (Current Research No. 2002-F7), Radiogenic age and isotopic studies: report 15. Geological Survey of Canada.
- Wodicka, N., St-Onge, M.R., Corrigan, D., Scott, D.J., Whalen, J.B., 2014. Did a proto-ocean basin form along the southeastern Rae cratonic margin? Evidence from U-Pb geochronology, geochemistry (Sm-Nd and whole-rock), and stratigraphy of the Paleoproterozoic Piling Group, northern Canada. *Geol. Soc. Am. Bull.* <https://doi.org/10.1130/B31028.1>.
- Yakymchuk, C., Kirkland, C.L., Clark, C., 2018. Th/U ratios in metamorphic zircon. *J. Metamorph. Geol.* 36, 715–737. <https://doi.org/10.1111/jmg.12307>.